ORIGINAL PAPER

Mesoporous Materials of the MCM Type: Synthesis, Application, use of Ionic Solids and Functionalization with Graphene: A Review

Paloma Truccolo Reato[1] · Adriele Sabrina Todero[1] · Fabiana de Oliveira Pereira[1] · Rogério Marcos Dallago[1] · Katia Bernardo-Gusmão[2] · Marcelo Luis Mignoni[1]

Abstract
The wide applicability of silica-based mesoporous molecular sieves in the most different scientific areas, such as catalysis, adsorption, drug delivery systems, sensors, CO_2 capture, enzyme immobilization, so on, is justified by their unique textural and structural characteristics. These materials exhibit high porosity, high specific surface area, limited pore distribution and controllable morphology what makes them adaptable and versatile. This review will address the latest in relation to molecular sieves of the M41S family, as well as their synthesis routes, highlighting the role of ionic solids and ionic liquids as structure-directing agents, the influence of heteroatoms addition (M^+/MCM), focusing on graphene incorporation (graphene/MCM), the means of characterization of these materials and their main applications. Considering the approaches that have been widely explored in the literature, it is safe to say that, depending on the synthesis route, these materials can be considered environmentally friendly, as it is possible to obtain them using clean reagents in one-pot syntheses. These materials already provide several solutions to nanoscale problems and its functionalization with graphene and the use of ionic solids and ionic liquids as SDA can further improve its performance.

Keywords Graphene · Ionic liquid · Ionic solid · Molecular sieves

1 Introduction

The development of materials is a multidisciplinary subject, which is practically fundamental to all scientific areas. In this review, mesoporous materials will be addressed, such as SBA and other types of mesoporous silica, but emphasis will be given to the MCM type, making a report since its discovery, going through the main characterization techniques, highlighting their applications and the new materials developed using the MCM structure as an object of study. An indicator, a WordCloud is shown in Fig. 1 with the most used terms throughout the text.

1.1 M41S Family Molecular Sieves

In recent decades, there has been a significant increase in research related to nanoscale materials due to their numerous possibilities of applications in the areas of catalysis, environmental pollution control, adsorption, separation, DDS (drug delivery systems), sensors, among others [1]. Among these materials are the so-called "molecular sieves", a concept developed by McBain in 1933 [2] which comprises porous solids that can selectively adsorb molecules which have a kinetic diameter of sufficient magnitude to allow their entry into the channels and cavities of the solid [3].

The IUPAC (International Union of Pure and Applied Chemistry) classifies molecular sieves according to their

✉ Marcelo Luis Mignoni
   mignoni@uricer.edu.br

   Paloma Truccolo Reato
   palomareato@gmail.com

   Adriele Sabrina Todero
   adrieletodero@hotmail.com

   Fabiana de Oliveira Pereira
   fabiana.opereira10@gmail.com

   Rogério Marcos Dallago
   dallago@uricer.edu.br

   Katia Bernardo-Gusmão
   katia.gusmao@ufrgs.br

[1] Universidade Regional Integrada Do Alto Uruguai E das Missões, Erechim, Rio Grande Do Sul, Brazil

[2] Universidade Federal Do Rio Grande Do Sul, Porto Alegre, Rio Grande Do Sul, Brazil

Fig. 1 WordCloud with the most used terms throughout the text

pore diameter (D_p) and therefore these can be: microporous ($D_p \leq 2$ nm), mesoporous (2 nm $< D_p \leq 50$ nm) or macroporous ($D_p > 50$ nm) [1].

Due to the need to process bulky molecules (size $> 0,75$ nm) in order to optimize industrial processes, in 1992 researchers from Mobil Oil Corporation developed a class of silica-based nanostructured mesoporous materials known as M41S. This family of materials covers several types of MCM (Mobil Composition of Matter of number n), the main ones being: MCM-41, which has a hexagonal structure and a unidirectional pore system; MCM-48, which has a cubic structure and three-dimensionally interconnected pores and MCM-50, which has a lamellar structure with layers of silica and double layers of surfactant [4–6].

Figure 2 presents the structures of MCM-41, MCM-48 and MCM-50 in a schematic form and their respective X-ray diffractograms with Miller indices and interplanar distances.

According to IUPAC, mesoporous silicas such as those in the M41S family encompass materials with pores, fissures, channels or cavities that are deeper than they are wide. Despite the reduced width, the depth of its pores allows the sorption of large molecules, justifying the wide range of applications of these materials. IUPAC also classifies zeolites, activated carbon and silica gel as porous materials [9].

In addition to the characteristics already mentioned, the variety of applications of these materials is also due to their high porosity, high specific surface area, limited pore distribution and controllable morphology. The possibility of controlling their syntheses in order to obtain the desired structure and pore size allows the adjustment of their properties for specific applications [10]. These characteristics imply the

insertion of molecular sieves in several advanced adsorption and catalysis techniques, as these materials are able to meet principles that are not achievable by older techniques [11].

The wide applicability of these materials is also directly linked to the properties that each structure gives them. MCM-41 and MCM-48 have high surface areas (1000–1500 m^2/g), good crystallinity (repeated and well-ordered grouping of their atoms) and high thermal stability, making them efficient for processes such as catalysis, separation and adsorption [12–14]. In addition, characteristics such as pore size (2–50 nm) and pore volume (>1.2 cm^3/g) also contribute to the efficiency of these materials for the mentioned processes [15, 16].

2 Synthesis of M41S Family Molecular Sieves

M41S family molecular sieves are synthesized in the presence of, among other reagents, a structure-directing agent (SDA) and a source of silica [4]. The SDA is composed of amphiphilic molecules which act as structure directors and, due to their ability to interact in a double way, form micelles that interact with the silicon oligomers and control the pore size [17, 18]. The use of organic structure directing agents forms organic-inorganic mesophases, attributing to these materials some of their innate characteristics [19]. The synthesis of these materials also requires the use of a mineralizing agent, which has the function of transforming the silicon-containing molecules into silicate ions (soluble species), the most used being NaOH and TMAOH (tetramethylammonium hydroxide), the organic cation of the last one also contributes to the formation of the basic units that make up silica [1, 18].

The properties of the materials of the M41S family are determined by the synthesis conditions employed, which may vary in the concentration of reagents, sources of silicon, pH of the solution, nature of the surfactant, time and temperature [20]. The most commonly used commercial silica sources are tetraalkoxysilanes (Si(OR)$_4$), as TEOS [(Si(OCH$_2$CH$_3$)$_4$)] and TMOS [(Si(OCH$_3$)$_4$)] [21], their molecular geometries are shown in Fig. 3. The pH of the reaction medium also influences the structure of the material: in basic media there is better condensation of silanol groups, resulting in a well-ordered structure with high specific surface area, whereas acidic media provide greater variation the morphology of mesoparticles [1].

When conducting the synthesis experiments of the M41S family of materials, the Mobil Oil Corporation researchers found that the composition of the synthesis solutions directly influences the final structure of the pores, as well as the diameter of the pores in MCM-41 increases as the length of surfactant chain

Fig. 2 Schematic representation of the structures of the mesoporous materials of the M41S family and their respective X-ray diffractograms: (**a**) MCM-41, (**b**) MCM-48 and (**c**) MCM-50. Source: Adapted from [6–8]
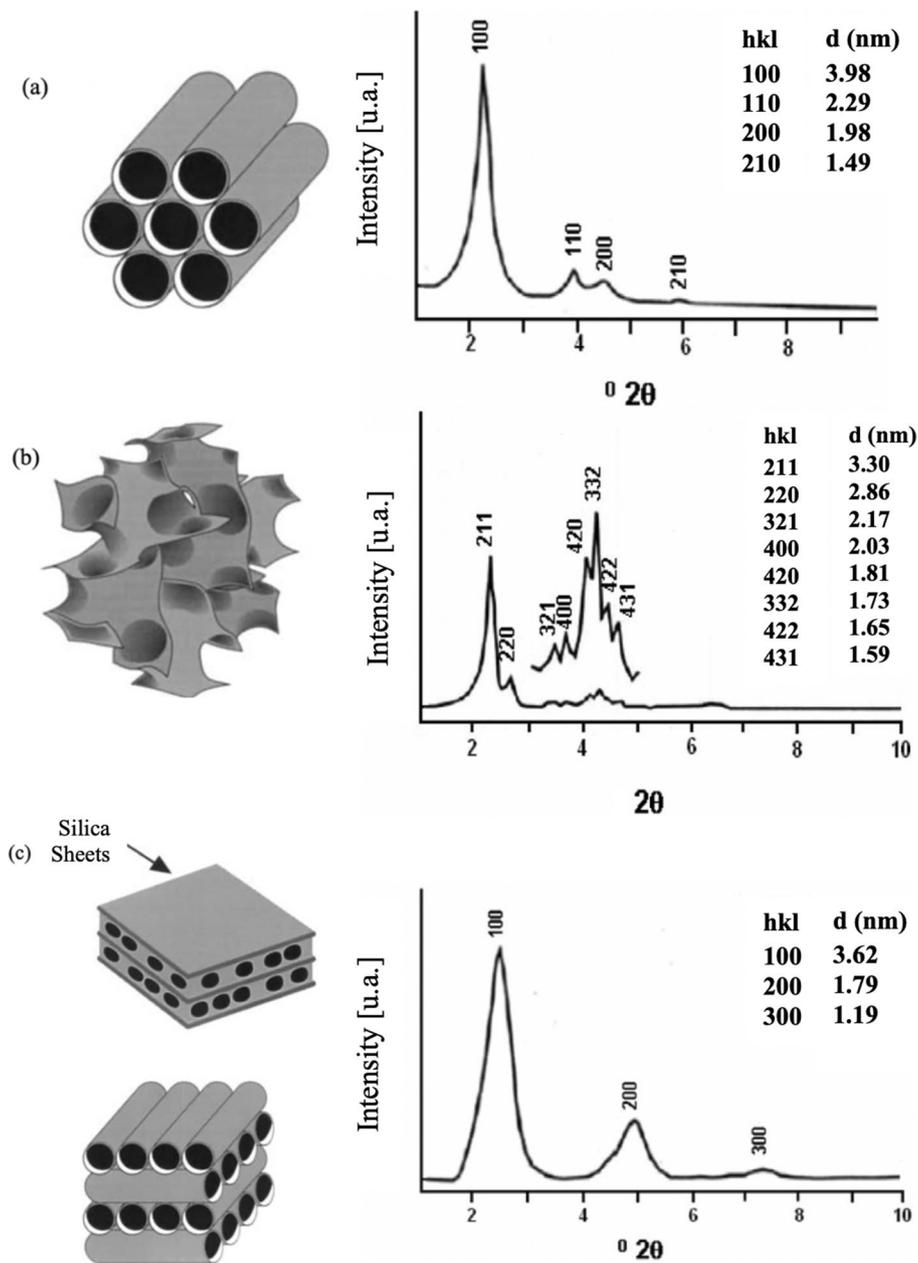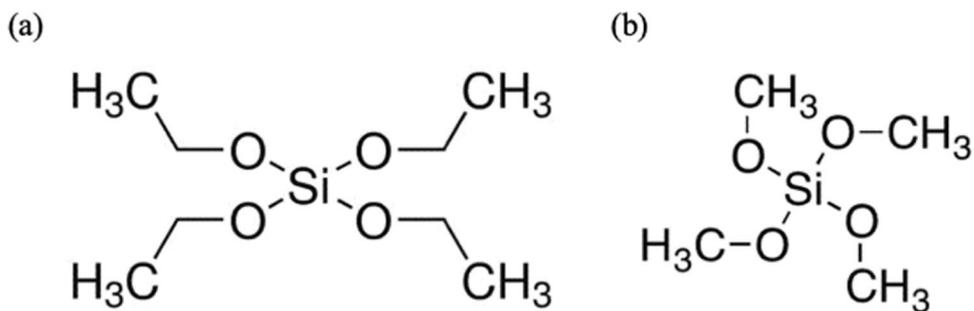

Fig. 3 Molecular geometries of (**a**) TEOS and (**b**) TMOS. Source: [22, 23]

increases [24]. For the synthesis, temperatures in a range between 100 and 150 °C were used for 24 to 144 h and the resulting solid after filtration, washing and drying was calcined at 540 °C under gas flow alternating between nitrogen and air, resulting in the mesoporous material [6, 25].

The most common means of synthesis are the sol-gel process [26], microwave heating [27], hydrothermal processing [28], template-assisted technique [29] and ultrasound [30]. A study report the synthesis of polysulfone/MCM-41 mixed matrix membranes and, for the molecular sieve synthesis, they used hydrothermal processing and the specific surface area of the material was 350 m^2g^{-1} [31]. MCM-41 was synthesized through the method of microwave irradiation of 90 and 120 W and obtained materials with surface areas of 1447.48 m^2g^{-1} and 1515.73 m^2g^{-1} and pore volumes of 1.12×10^{-6} m^3g^{-1} e 1.43×10^{-6} m^3g^{-1}, respectively [32].

Advances in research related to synthesis processes currently allow these to be conducted under milder experimental conditions and that alternative reagents are used, making them faster and less expensive. MCM-41 was produced using rice husk ash as an alternative source of silica, obtaining the material with a specific surface area of 848 m^2g^{-1} and pore volume of 0.84 cm^3g^{-1} [33]. MCM-41 and MCM-48 were obtained by performing the synthesis for 2 h without any heating and obtained materials with a surface area greater than 1000 m^2g^{-1} and pore volume greater than 1.0 cm^3g^{-1} [19].

There are several studies on the use of different structure directing agents, with CTAB (cetyltrimethylammonium bromide) being the most reported in the literature [34–36]. The use of ionic liquids (ILs) and ionic solids (ISs) as SDA has been the subject of several recent researches due to their ability to increase the space limits between the pores, making the material structure more stable and its crystallization thermodynamically possible [37]. In addition, characteristics such as non-flammability, adjustable polarity and solvation properties, low toxicity, high electrical conductivity and good thermal stability make these compounds attractive to both industry and academia [38].

2.1 Structure-Directing Agent

The structure director is a molecule composed of a hydrocarbon chain that has a polar (hydrophilic) and a nonpolar (hydrophobic) end in its structure [1]. In the reaction medium, these molecules act as a template and their addition leads to crystallization of a structure that would not form in their absence. In addition, they have the effect of filling pores, that is, their molecules provide greater structural stability to the mesoporous material [39–41].

The mesoporous structure is formed around these molecules due to the ability of their organic part to interact, through electrostatic, covalent bonds, hydrogen bonds or π ¬ π interactions, with the main groups of structure-directing agents and the ability to interact of its other part, which has an alkoxysilane that is capable of interacting with silica [42]. Therefore, the structure-directing agent and the silicate ions

form bonds organized in ordered sets favorable to the formation of the material [43].

It is important to clarify the distinction between the terms "structure directing agent" and "template", which can generate dubiousness when used. A structure directing agent induces the formation of a specific inorganic structure which would not form in its absence. The template is a substance which participates in the synthesis of the material and causes the substance to form around it. The same template will always form the same material [44].

2.1.1 Ionic Liquids and Ionic Solids

The growing concern with sustainability has encouraged research related to solvents that are less harmful to the environment, such as supercritical fluids, water, perfluorinated hydrocarbons and, recently, ionic liquids [45–47]. The terminology "ionic liquid" can generate dubiousness when used. Originally, these compounds were treated as "molten salts at room temperature", however, questioning the pertinence of the term "molten salts" and the definition of "room temperature", which can vary according to geographic location and time of year, these substances came to be called "ionic liquids". However, some compounds of an ionic nature have a melting point lower than 100 °C [48] and are solid at any ambient temperature. Therefore, when one of these substances is used at a temperature of synthesis at which it remains in the solid state, it should be called an "ionic solid". Nb-MCM type mesoporous material was synthesized using 1-tetradecyl-3-methylimidazolium chloride ([C_{14}MI] Cl) as SDA and it was reported as an ionic solid [37]. MCM-48 was synthesized for enzyme immobilization and the SDA [C_{14}MI]Cl was also reported as an ionic solid [49].

Ionic liquids have revolutionized research centers and the chemical industry in recent years [50, 51]. Its discovery was reported by Walden in 1914 [52] while looking for liquid molten salts at temperatures at which it would be possible to use his equipment without major adaptations. In this research, motivated by the relation between the molecular size and the conductivity of molten salts, he discovered the compound [EtNH$_3$][NO$_3$], which has a boiling temperature of 12 °C [53]. Since that time, numerous ionic liquids have been developed and used in several areas of research, which include the synthesis of mesoporous molecular sieves. Table 1 presents some ionic liquids reported in the literature for the synthesis of mesoporous solids.

These structure-directing agents present an organic cation, which promotes the physical properties of these substances, and an anion, which can be organic or inorganic and is responsible for controlling chemical properties and interactions [57]. In view of this, ILs can be synthesized in order to fulfill specific functions and, for this reason, they are called designer solvents. Its characteristics are regulated

Table 1 Ionic liquids reported in the literature for the synthesis of mesoporous materials

Abreviation	IUPAC nomenclature	Molecular Formula	Synthesized material	Reference
[C$_{16}$MIM]Br	1-Hexadecyl-3-methylimidazolium bromide	C$_{20}$H$_{39}$BrN$_2$	MCM-41	Zhang et al. [54]
[bMIM][Ac]	1-Butyl-3-methylimidazolium acetate	C$_{10}$H$_{18}$N$_2$O$_2$	MCM-41 SBA-15	Mohamedali et al. [55]
[pMIM][Tf2N]	1-propyl-3-methylimidazolium bis(trifluoromethylsulfonyl)imide	C$_9$H$_{13}$F$_6$N$_3$O$_4$S$_2$	MCM-41 SBA-15	Mohamedali et al. [55]
[C$_{14}$MI]Cl	1-Tetradecyl-3-methylimidazolium chloride	C$_{18}$H$_{35}$ClN$_2$	Nb-MCM-41 Nb-MCM-48	Bordin et al. [37]
[C$_{16}$MI]Cl	1-Hexadecyl-3-methylimidazolium chloride	C$_{20}$H$_{39}$ClN$_2$	ZSM-5/MCM-48 ZSM-35/MCM-48 ZSM-55/MCM-41 ZSM-35/MCM-41	de Aguiar Pedott et al. [56]
CTAB	Cetyltrimethylammonium bromide	C$_{19}$H$_{42}$BrN	MCM-41 SBA-16	Renuka et al. [34]
CTAB	Cetyltrimethylammonium bromide	C$_{19}$H$_{42}$BrN	MCM-41	Vyshegorodtseva et al. [35]

by the selection and combination of cations and anions [58], as well as by the processes of synthesis, the most common being acid-base neutralization and salt metathesis [59, 60].

These substances remain in the liquid state below 100 °C or even at room temperature [51, 61]. This is due to the large difference in molecular size between cations and anions, causing the molecules that make up these substances to be weakly bonded to each other. There are two main groups of ionic liquids: those composed of the imidazole organic molecules (cation of the imidazole compound of formula C$_3$H$_4$N$_2$) and pyridinium (cation of the pyridine compound of formula C$_5$H$_5$N). The structure of these groups is shown in Fig. 4. Several ions can be used to compose the ILs, the most common anions being the BF$_4^-$, BF$_6^-$, Br$^-$ and Cl$^-$, plus larger complexes such as ethyl sulfate, tetrafluoroborate or hexafluorophosphate [51, 62].

The complex interactions of Coulomb, van der Waals and hydrogen bonds make the physical properties (solubility, melting point, viscosity, density and hydrophobicity) of ILs adaptable and, therefore, these solvents are able to meet a wide range of processing requirements [63]. Ionic liquids and solids are prominent for their low vapor pressure, which provides high thermal stability and good conductivity [64]. The ILs derived from the imidazole cation are of interest because of the presence of hydrogen bonds, due to their high molecular ordering [65, 66] and because they provide a structure that, by changing the position of the anionic chains, allows the adjustment of physical and chemical properties [67, 68].

Another advantage of ILs resulting from the non-detectable vapor pressure under normal conditions is that they do not contribute to the amount of volatile organic compounds

Fig. 4 Ionic liquids and solids with (a) imidazole and (b) pyridinium cations. Source: [51]
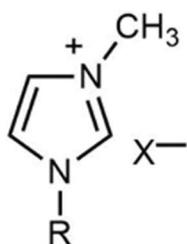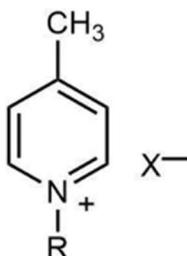
(VOCs) in the atmosphere, as well as non-toxicity by inhalation in humans and animals [69]. Furthermore, these substances are industrially interesting for the amount of potentially possible compounds: at least thousands of pure compounds, a billion binaries and 10^{18} ternary mixtures [70]. ILs have been used for different purposes, such as: product manufacturing (catalysis, medicine, plastics), processes (mineral extraction, separation and adsorption, CO_2 capture, cellulose treatment, biomass processing), electrochemistry (batteries, supercapacitors), materials (metals, nanotubes, graphene) and transport (lubricants, fuels) [65, 71].

As already seen, the SDA is the determining reagent for the formation of the structure of mesoporous materials and ILs have proven to be fruitful in this function. Hierarchical zeolite/MCM materials (MCM-48 and MCM-41) were produced using the ionic solid [C_{16}MI]Cl as a structure directing agent at room temperature with a synthesis time of, respectively, 24 h and 2 h, with MCM-41 being the material that presented the highest specific surface area equal to 855 m^2g^{-1} [56]. Micro-mesoporous MCM-41 was synthesized using CTAB and three different ionic liquids as co-templates: n-butyl-DABCO bromide ([N-buDabco]Br), n-butylpyridinium bromide ([N-bupy]Br) and n-butyl-hexamethylenetetramine bromide ([N-buHMTA]Br), the first one resulting in the material with the highest specific surface area equal to 1035 m^2g^{-1} [72]. The synthesis of the MCM-41 mesoporous material and the disordered mesoporous molecular sieve KIT-1 were described using the ionic liquid hexadecyl-4-aza-1-azoniabicyclo[2-2-2]octane bromide (IL-C_{16}) as a template and, with specific surface areas of 1221 m^2g^{-1} and 1012 m^2g^{-1}, respectively [73].

3 Functionalization of MCM Type Molecular Sieves

The amorphous nature of the pore walls of pure MCMs causes them to have relatively low catalytic and sorption activities, limiting their extensive applications [74]. The incorporation of heteroatoms in the structure of MCMs is a way of controlling the characteristics of these materials and, therefore, synthesizing them with previously established properties and specific purposes. Depending on the desired application, these modified molecular sieves can generate basic or acidic sites with specific hydrothermal properties [75, 76].

The structure of MCM-41 in its pure form (silica only) has a neutral network [18]. When, for example, an atom of aluminum, which has an oxidation state of +3, replaces a silica atom with oxidation state +4, a residual negative charge that can be neutralized by counter-ions is generated [18]. The incorporation of multivalent metal ions (Co, Zn, B, Al, Ga, Cr, Fe, Ti) in the structure of these materials results in mesoporous catalysts with redox or acid-base properties [77].

The manipulation of the MCM structure with the addition of heteroatoms can favor different types of reactions [18]. Heteroatom modified (Fe, Ce, Zn, Mg) MCM-41-silica carriers were synthesized for Lomefloxacin delivery systems by ion-exchange approach and the materials exhibited good features such as high specific surface area (510–813 m^2/g), an ordered pore framework and uniform distribution of heteroatoms [78]. Mesoporous molecular sieves MCM-41 and Co-MCM-41 were produced by hydrothermal synthesis method to denitrogenation from model fuel and diesel oil and the pore volumes and surface areas of MCM-41 and Co-MCM-41 were, respectively, 0.76, 0.53 m^3/g and 986, 637 m^2/g [79].

Ce-MCM-22 were synthesized by hydrothermal method and evaluated its enhanced catalytic performance for the removal of olefins from aromatic stream [80]. Titanium and chromium containing MCM-48 were synthesized by in situ modification method and studied its catalytic activity for styrene oxidation using H_2O_2 as oxidant [81]. Al-containing pore-expanded MCM-41 was produced from rice husk ash and loaded them with polyethyleneimine to produce adsorbents for CO_2 capture [82]. A series of H-MCM-22 with different Si/Al ratios wew synthesized and its performance was evaluated for the conversion of methanol to hydrocarbons [83].

Graphene has been subject of several researches due to its excellent electronic, biomedical and mechanical properties [84]. The incorporation of graphene in materials of the M41S family results in a graphenesilicate which can be a very promising mesoporous material in applications in the areas of adsorption and catalysis.

3.1 Incorporation of Graphene in MCMs

Graphene is an advanced carbon nanomaterial first identified in the early 1960s, however, it was separated from the monolithic system only in 2004 by Novoselov using micro-computer peeling (Scotch-tape method), which challenged the scientific understanding of two-dimensional crystals [85, 86]. The structure of graphene consists of a single sheet of carbon atoms packed in a hexagonal lattice. The atomic structure of this material serves as a platform for other carbon structures, such as fullerenes, nanotubes and graphite itself [87, 88].

The structure of graphene is very stable and the bond length between carbon atoms is only 0.142 nm [89]. In addition, it has a high surface area, with a theoretical value of 2630 m^2g^{-1} [90]. When an external force is applied, the graphene surface compensates for deformation, with no rearrangement and misalignment between atoms, keeping the structure consistent and stable [91]. Due to these and other properties of graphene, this material comprises a wide range of applications in the energy field [92, 93], catalysis [94], drug delivery systems [95], adsorption and separation

of gases [96], green chemistry [97], supercapacitors [98], biosensors [99], batteries [100], solar and fuel cells [101, 102], among others.

The global graphene market consists of three major products which are determined according to the synthesis process: graphene nanoflakes (non-oxidized), graphene oxide or reduced graphene oxide, and graphene films. These materials have different characteristics in terms of impurities, yield, uniformity of size and thickness, production costs, applications, among others [103]. Pure graphene has low water solubility, so the main reason for inserting epoxy, hydroxyl and carboxyl groups into its structure in order to obtain graphene oxide is to make it highly hydrophilic and, therefore, to increase the range of applications of the material in this sense [104].

From 2022 onwards there are some studies reporting the synthesis of graphenesilicates: a material called MRD-1, a MCM topology graphenesilicate [105], MRD-2, a graphenesilicate doped with niobium [106], MRD-3, a graphenesilicate doped with titanium [107], MRD-4, a graphenesilicate doped with titanium zinc [108], MRD-5, a graphenesilicate doped with iron [109] and MRD-6, a graphenesilicate doped with aluminum [110]. All the cited materials use an ionic solid ([C$_{16}$MI].Cl) as SDA. The advantages of the synthesis method of all these materials are that it can be carried out in room temperature and the fact that graphene is incorporated in situ into the solid structure of the MCM topology makes this process technically and commercially attractive. The process for obtaining this new graphenesilicate material (MRD-5) is represented in Fig. 5.

4 Characterization of Solid Materials

In this section, the following methods of characterization of solid materials will be discussed: X-ray diffractometry (XRD), textual analysis of nitrogen adsorption/desorption, scanning electron microscopy (SEM), transmission electron microscopy (TEM) and thermogravimetry (TGA).

4.1 X-ray Diffractometry (XRD)

According to its atomic organization, a solid material can be defined as amorphous or crystalline. Crystalline structures present periodicity and ordering, a condition that does not occur in amorphous materials [111]. Understanding matter at the atomic level, that is, knowing the arrangement of atoms in molecules and crystals, is essential for understanding the chemical, physical-chemical and biological properties of compounds [112]. For this purpose, it is necessary to employ techniques that provide information at the atomic resolution level and, even if indirectly, the characteristic images of different crystalline solids [113]. Among the existing techniques for the characterization of crystalline structures, X-ray diffractometry is among the most relevant [112].

X-rays were discovered in 1895 by Wilhelm Conrad Röntgen (1845 – 1923) while studying the fluorescence of compounds using cathode ray tubes [114]. In 1912, Max von Laue (1879–1960) theoretically predicted and experimentally proved that X-rays were diffracted by crystals [115, 116].

Fig. 5 Graphical representation of the mesopore graphenesilicate material MRD-5 synthesis. Source: author

X-rays are efficient in this type of analysis because they have a wavelength compatible with that of electrons and with interatomic distances (on the order of 150 pm) and, therefore, can be satisfactorily applied in the exploration of dimensions with this order of magnitude [117]. X-ray diffractometry became truly relevant in the determination of crystalline structures from 1912, when William Henry Bragg (1862–1942) and William Lawrence Bragg (1890–1971) proposed a simple and efficient method to conduct the technique, experimentally determining the crystalline lattice of KCl and NaCl [118].

When X-rays fall on a solid, they are scattered by the electron layers of the atoms which make up the material's structure. The phenomenon of diffraction is represented by the wave beams reflected by two subsequent planes. When there is regular spacing (crystalline lattice) between atoms located in different planes of a solid and the incident radiation has a wavelength (λ) in the order of the spacing between the crystalline planes, the waves will be in phase and, therefore, will interfere constructively [14]. This phenomenon is graphically represented in Fig. 6.

Trigonometrically analyzing the phenomenon represented in Fig. 7, in 1913 William Lawrence Bragg and William Henry Bragg proposed Bragg's Law (Eq. 1), which is a simple equation that relates the wavelength of X-rays, the interatomic spacing and the diffraction angle for constructive interference. If Bragg's Law is not satisfied, the interference will be non-constructive in nature and the diffracted beam produced will be of very low intensity [14, 117].

$$n\lambda = d_{hkl}sen\theta + d_{hkl}sen\theta = 2d_{hkl}sen\theta$$
$$n = 1, 2, 3 \ldots$$

(1)
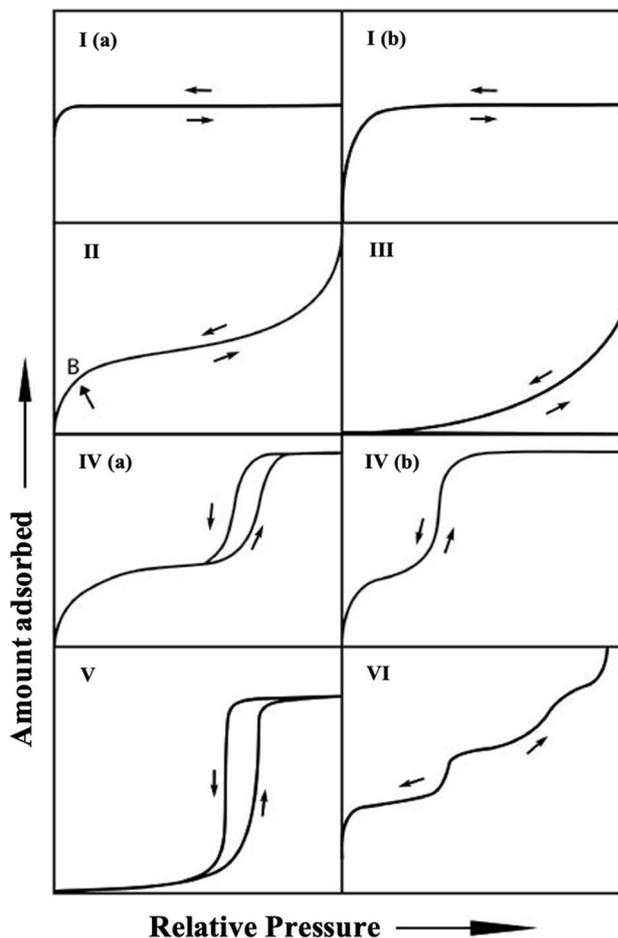
Fig. 7 Classification of adsorption isotherms according to IUPAC. Source: [119]

Fig. 6 X-ray diffraction by planes of atoms (A–A' and B–B'). Source: [14]
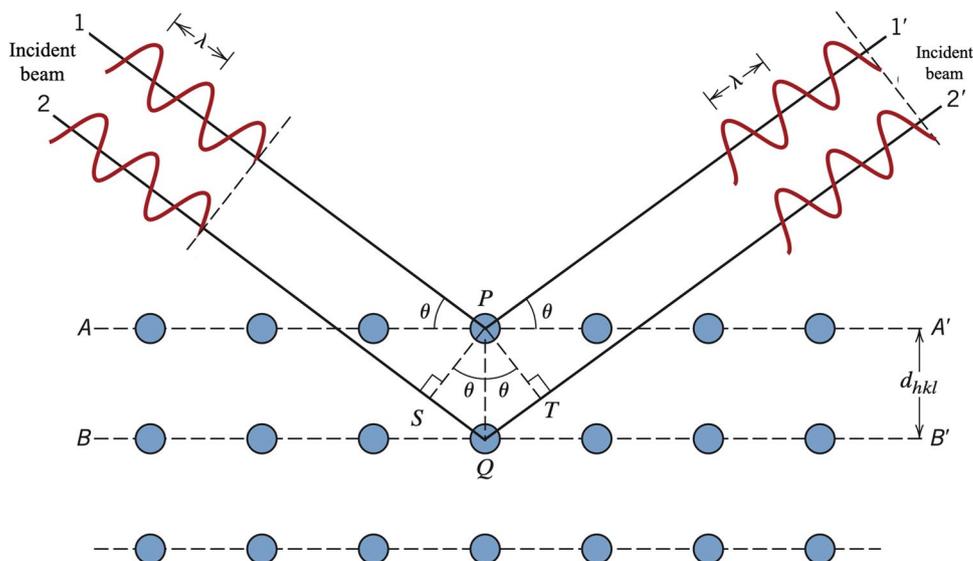
where n is the order of reflection, λ is the wavelength of X-rays, d_{hkl} is the interplanar spacing depending on the Miller indices (*h*, *k* e *l*) and θ is the angle of incidence of the X-ray waves.

In general, the operation of the equipment used in this technique consists of the generation of electrons by the thermionic effect in a tungsten filament, which are accelerated towards the anode by a significant difference in potential (30 to 60 kV). X-rays are generated at the anode and exit the generator tube through the beryllium window, which filters the continuous spectrum (*Bremsstrahlung*, in German) and therefore causes them to pass through only waves in the characteristic X-ray spectrum (defined λ) [120]. The detection of the diffracted X-rays is done by a radiation detector and the response is given in a diffractogram composed of the ratio between the angle of incidence/diffraction (2θ) and the intensity of the characteristic peak of the solid.

From Bragg's Law (Eq. 1) it is possible to calculate the theoretical positioning of the characteristic peaks of crystalline solids [121] and relate these data with those obtained in the application of X-ray diffractometry.

4.2 Textural Analysis of Nitrogen Adsorption/Desorption

The specific area of a solid can be defined by determining the amount of an adsorbate, usually a gas, needed to coat the surface of an adsorbent with a mono or multilayer [122, 123]. When a solid comes into contact with a gas or vapor in a closed system at constant temperature, the solid physically or chemically adsorbs the gas and, as an effect, its mass increases and the gas pressure decreases until both reach constant values. The amount of gas that has been adsorbed by the solid can be determined by the decrease in pressure from the application of the gas law or by the total mass of gas that has been adsorbed [123].

The surface area of solids can be calculated by the method of Langmuir or of Brunauer, Emmett and Teller (BET) from the isotherms of adsorption/desorption of nitrogen (N_2) at the boiling point of the gas (77 K). The choice of method depends on which type of adsorption layer the pore size of the solid supports: BET for multilayers and Langmuir for monolayers [122]. Other gases can be used for this purpose, such as argon (Ar), carbon dioxide (CO_2) and organic vapors (dynamic vapor sorption) [124]. In addition to the surface area, this analysis also allows determining the pore distribution of the material using methods based on Kelvin's equations, which relate pore size to condensation pressure or capillary evaporation [125–127].

As already seen, the answer of this analysis is provided by the adsorption/desorption isotherms of N_2, which relate the molar amounts of adsorbed gas according to the variation of the relative pressure (P/P_0). Adsorption isotherms depend on the porosity of the material and, according to IUPAC, are classified into six types which are shown in Fig. 7.

The exact shape of the isotherms is strongly influenced by the choice of adsorbate [128]. Type I isotherms correspond to microporous solids with low external surfaces, and isotherm I (a) is related to microporous solids with narrow pores (<1 nm) and isotherm I (b) with larger pores (< ~ 2.5 nm). On the other hand, type II isotherms correspond to non-porous or macroporous structures, which normally present a linear phase and a concave phase up to point B (indicated in Fig. 8, II), at which the monolayer is filled. Similarly, type III isotherms correspond to non-porous or macroporous materials, however, they do not present point B on the adsorption curve, that is, the monolayer is not formed due to the weak interaction between the solid and the gas, generating accumulations of gas in more favorable locations of the solid [119].

The type IV isotherm is related to mesoporous materials and, in these solids, the pore size strongly influences the isotherm formed: isotherm IV (a) is characteristic of solids which have pore widths greater than the critical, which depend on temperature and adsorption system, and isotherm IV (b) corresponds to mesoporous systems that have pores with widths smaller than system criticism. Type V isotherms resemble type III isotherms, which can be attributed to the weak interactions between the gas and the solid. Finally, type VI isotherms correspond to solids with extremely homogeneous structures that present non-porous surfaces, in which the different levels are related to successive adsorbed layers [119].

The adsorption and desorption curves that compose the isotherms usually do not coincide, this is due to the difference between the saturation pressures generated by the phenomena of condensation and evaporation inside the pores. This causes the formation of hysteresis, which present patterns that depend on the characteristics of the pores of the analyzed solid. Figure 8 presents the IUPAC classification for hysteresis phenomena, with each of these six types being strongly related to particular characteristics of the underlying adsorption mechanism and pore structure [119].

Hysteresis classified as H1 are related to materials which have narrow mesopores, characteristic of silicon-based materials, such as those of the M41S family. H2-type hysteresis corresponds to materials that have a complex pore structure, in which pore interconnection effects play an important role and are subdivided into: H2 hysteresis (a) related to very steep desorption branches, which occur due to blockage or percolation of narrow pores and H2 hysteresis (b) in which there are also blocks, however, related to larger pores. These isotherms occur in ordered mesoporous materials such as SBA-16 and KIT-5 silicas [119].

Fig. 8 Classification of hysteresis according to IUPAC. Source: [119]
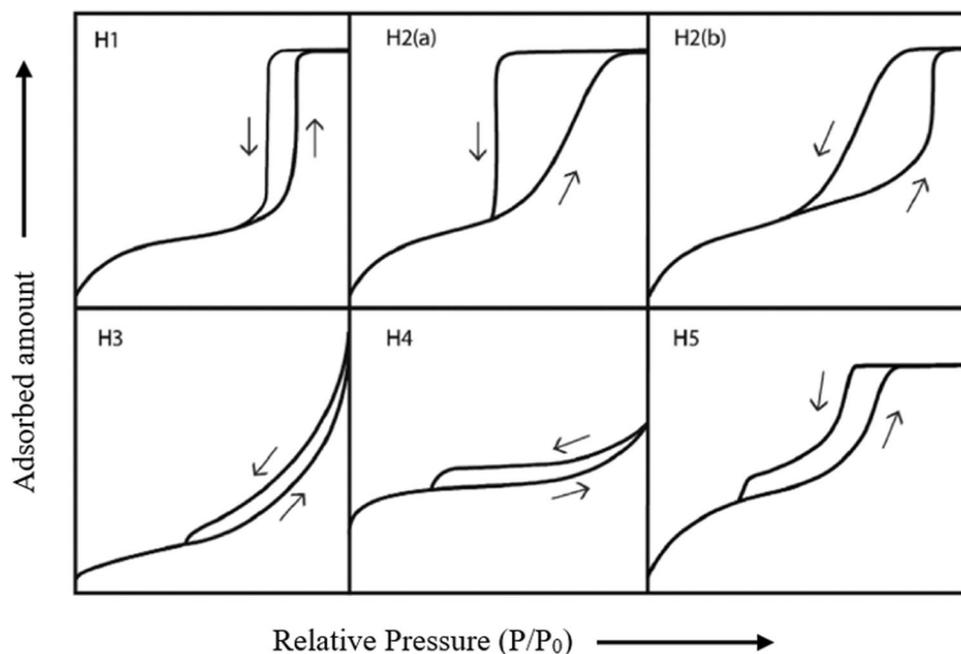
Type H3 hysteresis corresponds to materials in the form of plates with a non-rigid macroporous structure in which there is no total pore filling. This hysteresis is normally associated with clays. H4-type hysteresis occurs in micro and mesoporous aggregates, in which only the microporous phase is filled and appears in the analysis of zeolitic structures and micro-mesoporous coals. Finally, H5 hysteresis is uncommon and occur in mesoporous structures with open or partially closed pores, characteristic of silica-based materials with a hexagonal structure [119].

4.3 Scanning Electron Microscopy (SEM)

The maximum resolution limit of optical microscopes, which illuminate the object of interest with visible light or ultraviolet light, is determined by the diffraction effects resulting from the wavelength of the light used. Therefore, this type of microscope is limited to a magnification of 2000 times and, above this value, smaller details become imperceptible. In order to increase the resolution of a microscope, it is possible to use a light source with a shorter wavelength than that presented by visible light. In view of this, the scanning electron microscopy (SEM) technique uses, instead of photons as in a conventional optical microscope, an electron beam, solving the resolution problem caused by the white light source. Thus, SEM allows the visualization of the morphology of solid materials with resolutions between 2 and 5 nm for commercial equipment or 1 nm for advanced research equipment [129].

In SEM, therefore, a thin electron probe with energy generally between 1 and 30 keV is generated under vacuum [130], pointed at a sample and scanned along a pattern of parallel lines. As a result of the impact of the incident electrons, secondary electrons and/or backscattered electrons are generated [129] and, from these, serial signals are collected by a detector, which is synchronized with the known location of the beam in the sample. The signal strength value is used to modulate the corresponding image pixel and these are combined in order to form an image with dimensions and pixel distribution which depend on the chosen raster pattern [131].

For a good response to be obtained, the sample submitted to SEM must have a conductive profile due to the need for interaction between the electronic beam and the sample. If this does not happen, it is possible to make it conductive through physical processes such as evaporation or sputtering. Furthermore, when ionic layers are deposited in the sample, the level of electron emission can be optimized and this will contribute to the construction of the image. The most commonly used metal ions for this purpose are gold (Au), gold-palladium alloy (Au-Pd) and platinum (Pt) [132].

4.4 Transmission Electron Microscopy (TEM)

Transmission electron microscopy is considered one of the most important techniques to obtain direct structural information of porous materials at a nanometer scale. The difference between SEM and TEM is that while in SEM the detectors are positioned on the same side of the sample as the incident beam in order to detect scattered secondary electrons, in TEM the detectors are positioned behind the

sample in order to detect transmitted electrons through a very thin sample of material (less than 100 nm) [133].

The operation of a conventional transmission electron microscope consists of, as already mentioned, irradiating a sample of nanometer thickness with a beam of electrons of uniform current density, with the electron energy generally maintained around 100 keV [134]. The image is a result of the diffraction contrast. In this analysis, the sample must be oriented so that part of the electron beam is transmitted and part is diffracted. The image of the sample is formed simultaneously with the passage of the light beam through it and only the transmitted electrons are analyzed by the detector being translated into a mixed image signal. Magnification of the image is obtained by lenses underneath the sample which project the image formed by the electrons onto a recording device. The magnification is defined by the optical system and the resolution for aberrations in lens performance [135].

The hexagonally ordered mesoporous structure of MCM-41 and the cubic ordered mesoporous structure of MCM-48 could only be observed and determined by the advent of TEM, proving the importance of this analysis and how much it can be decisive in a study [136].

4.5 Thermogravimetry (TG)

Thermogravimetry (TG) or thermogravimetric analysis (TGA) is a thermoanalytical technique conducted on a thermobalance which evaluates the variation of the mass of a sample as a function of temperature or time, in which the temperature is kept constant during the analysis. The results of this technique are quantitative and depend on the thermal decomposition of volatiles present in the sample or on the incorporation of atoms or molecules from the gases that make up the atmosphere conducting the test, respectively decreasing or increasing the mass of the analyte [137].

The thermobalance or thermogravimetric analyzer is composed of an electronic microbalance, an oven, a temperature programmer and a computer which allows the coordination of the analysis, so that the sample is simultaneously weighed and heated or cooled in a controlled manner and the mass, the time and temperature are weighted [138]. The temperature programmer can include heating, cooling, isothermal holds, or a combination of these factors [139]. The test atmosphere determined by the gas used can be inert, oxidizing or reactive [140] and its moisture content can vary from dry to saturated [141].

This analysis is used in order to know parameters related to the composition, degree of curing and thermal stability of a material, the latter being determined by the specific temperature or time limit to which the material can be subjected without significant loss of its properties [142, 143].

5 Applications

The use of molecular sieves in both research and industry has increased exponentially in the last years. As already mentioned, mesoporous silicas are regarded as very versatile materials and the possibility of precise and easily control its pore shapes and sizes makes these materials of great interest in many areas of modern science and technology [144, 145].

Many applications of M41S family materials are reported in the literature, such as depolymerization [146–149], CO_2 capture [150–154], enzyme immobilization [37, 155–157], drug delivery systems [158–161] and catalysis [162–165]. The most common applications of the M41S family of materials are presented below.

5.1 Catalysis

Catalysts play a crucial role in many chemical reactions and new compounds with catalytic properties are needed for sustainable chemical production [166, 167]. Among conventional supports such as Al_2O_3, ZrO_2, CeO_2, mesoporous materials (SBA-15, MCM-41 and SBA-16) are being widely investigated and proving to be promising materials for heterogeneous catalysis [168].

Pure MCM-41 mesoporous silica with active mesoporous sites was applied as a highly efficient and recoverable catalyst for the synthesis of α-aminonitriles and imines. The authors highlighted the simple work-up procedure, excellent yields, short reaction times and the non-use of toxic solvents [169]. Al-MCM-41 (Si/Al = 30) using CTAB as SDA and tetrapropylammonium hydroxide (TPAOH) as a co-surfactant additive were synthesized as a catalyst for the dehydration of methanol to dimethyl ether (DME). The best conversions were 72% and 73% performed by CTAB/TPAOH of 0.75 and 0.20, respectively [170].

The catalytic activity of different active metals (Li, La, Ce, Mg, K) impregnated on MCM-41 was explored for transesterification of glycerol into glycerol carbonate and 5 wt% Li incorporated MCM-41 proved the better catalytic activity [171]. MCM-41 modified by transition metal oxides (molybdenum, vanadium and tungsten) were synthesized for the removal of sulfur compounds in real and model fuels by oxidative desulfurization. Mo-MCM-41 and W-MCM-41 were the most effective, dibenzothiophene was removed completely and sulfur removal in gasoline and diesel fractions reached 91 and 63%, respectively. Furthermore, the catalysts still had activity in gasoline fraction desulfurization even after 5 cycles [172].

Phosphotungstic acid (PTA)/MCM-41 catalyst was synthesized for ultrasound-assisted depolymerization of lignin and the conversion of the reaction was 94.79% under optimum conditions of an ultrasound frequency of 30%,

temperature of 300 °C and reaction time of 6 h [173]. MCM-41 derived from coal fly ash modified with molybdenum was studied as a catalyst for the oxidative desulfurization of dibenzothiophene (DBT). The authors achieved a 94% of DBT removal by optimizing the influencing parameters of the process [154].

5.2 Enzyme Immobilization

Enzymes are biological catalysts with wide applicability in many industries like food products, textile, biochemical, biosensors and pharmaceutical due to their high specificity and effectiveness when compared with chemical catalysts [174]. The mechanical and chemical properties of the support and the high selectivity of reactions involving enzymes directly influence their fixation onto inorganic materials [175]. In recent years many supports such as polymers, mesoporous materials, nanofibers, membranes, nanomaterials and cellulose have been studied and improved leading to better enzyme/supports interactions [176].

Among the countless possibilities of supports, MCM-41 has highly suitable structural characteristics for the immobilization of enzymes [19]. The large pores of this material allow the bulky molecules of the enzyme to diffuse into them. In addition, the silanol groups present on the surface of MCM-41 facilitate the binding of the enzyme to the support via hydrogen bonds. Furthermore, the enzyme inserted in a well-defined space prevents its denaturation and can increase its stability [177].

Nb-MCM-Type mesoporous materials using MCM-41 and MCM-48 were synthesized for in situ lipase immobilization and obtained materials with surface area of 954 and 704 m^2/g for Nb-MCM-41 and Nb-MCM-48, respectively. Furthermore, the supports enabled a high number of recycles (26 recycles with a residual activity of 49.62% for Nb-MCM-41 and 16 recycles with a residual activity of 53.01% for Nb-MCM-48) in successive esterification reactions and excellent storage stability (5 months) [37]. Organosilane-modified Fe_3O_4@MCM-41 was prepared and applied as support for L-ASNase covalent immobilization. The immobilized enzyme exhibited excellent reusability (56.3% activity after 12 cycles), higher affinity for substrate than native L-ASNase and significant storage time (54% and 26% of the initial activity after storage at 4 and 25 °C) [174]. Trypsin was adsorbed in pure and functionalized (N-(2-aminoethyl)-3-aminopropyl and aminopropyl) SBA-15 and the final compound was applied as an enzymatic bioreactor for protein digestion and, 1 min after the protein was added to the trypsin-immobilized mesoporous support, fragments of myoglobin could already be seen giving a 100% sequence coverage [178].

MCM-48 mesoporous support was synthesized for in situ *Candida antarctica* lipase *B* (CALB) immobilization and it exhibited a residual activity above 50% when stored under refrigeration for 75 days and it was possible to reuse the catalyst for up to 10 cycles with residual activity of approximately 50% in an esterification reaction using oleic acid and ethyl alcohol [49]. CALB was also immobilized in G-MCM-41 (glutaraldehyde/MCM-41) amino-modified with 3-aminopropyltriethoxysilane and applied as a reaction catalyst in the transesterification of soybean oil and phytosterol. The immobilization efficiency reached 93%, the residual activity was 83% after 7 reuses and it exhibited >50% of activity after stored for 40 days at 4 °C [179].

5.3 Bionanotechnology

With the development of nanotechnology, materials science increasingly needs to understand the detail of the design of some materials at the nanoscale in order to obtain desired nanostructures and, therefore, with specific performances. In the area of bionanotechnology, there are currently several types of nanomedicines successfully used in the treatment of numerous diseases, as well as molecular sieves are used in drug delivery systems (DDS), which consist of a polymeric matrix from which a drug is gradually released under appropriate conditions [180, 181].

There are studies reporting the use of mesoporous silica in nanodynamic therapies which, activated by infrared light, microwaves, ultrasound, X-rays or by an internal chemical/biological reaction in the tumor microenvironment, generate in situ free radicals/reactive oxygen species in order to treat deep tumors [182]. Immunotherapy is another resource for cancer treatment by stimulating the patient's immune system and silica-based mesoporous materials are also being applied in vaccines, immune cell recruitment and immunological cell death/combinatorial therapy [183]. Besides cancer immunotherapy, mesoporous silica are also used in other cancer-related applications such as diagnostic, brain targeting, theranostic and gene therapy [180].

Mesoporous silica and metal–organic frameworks (MOFs) are also reported as photosensitizers used in photodynamic therapy to produce reactive oxygen species that are effective in destroying cells and therefore can be applied to treat skin and eye diseases as well as certain types of cancer [184]. Silica-based nanovehicles are gaining space in photoactivated cancer therapy due to light dosage and adjusted therapeutic area, as well as milder side effects when compared to monotherapy [185]. Silica nanoparticles are also used as theranostic nanoplatforms and they provide many advantages when compared to other similar systems for precise cancer diagnosis, stimuli-triggered drug delivery and tissue bio-adhesive materials [179].

Several mixtures of polymers and polymer-based composites, such as bioactive glasses and ceramics, have been

used for this purpose. In this case, the drug can be deposited by means of direct compression, mechanical mixture matrix/drug or wet granulation. The disadvantage of these methods is that in heterogeneous matrices it is not possible to guarantee a homogeneous distribution of the drug through the matrix and it can affect the release rate. Therefore, the use of chemically homogeneous materials with well-defined porosity in terms of volume and size can solve this problem [186].

Thus, the pore arrangement of molecular sieves makes these materials suitable for use in drug delivery systems (hosting and further delivering) of a variety of molecules of pharmaceutical interest [187]. MCM-41 with different groups (amino, chloro and glycidoxy groups) were evaluated as a drug delivery system for acetylsalicylic acid and the MCM-41/glycidoxy group was the most favorable for this purpose [188]. Pure MCM-41 and MCM-41 functionalized by 3-aminopropyltriethoxysilane grafting was evaluated for Ibuprofen-controlled release and the last one showed the best results [189]. MCM-48/hydroxyapatite composite was also synthesized for ibuprofen-controlled release and it was concluded that the material offers a significant potential for controlled drug delivery systems [190].

The potential of MCM-41 and Hollow Mesoporous Silica (HMS) were studied as DDS for anticancer drug bicalutamide (BLT) and concluded that both materials increased in vitro antitumor activity against prostate adenocarcinoma LNCaP cells and provided good safety and more reliable drug bioavailability [191]. Ofloxacin@Doxorubicin-Epirubicin functionalized MCM-41 nanocarriers were synthesized as synergistic drug delivery tools for cancer related bacterial infections and MCM-41 loaded with the epirubicin (anticancer drug) and ofloxacin (antibiotics) was the most effective formulation [192].

Mesoporous silica nanoparticles are also reported as promising nanocarriers for pulmonary drug delivery, overcoming anatomical, immunological and physiological barriers of the respiratory system and are proving to be an effective alternative in the treatment of lung cancer and asthma [193]. Still in relation to pulmonary diseases, mesoporous silica nanoparticles loaded with dexamethasone and capped with a peptide to avoid cargo leakage are being studied as an alternative treatment for acute lung injury [194]. Regarding to capping agents, a study dedicated to evaluate its properties in order to integrate pore-capping, drug-loading and tumor-targeting abilities in mesoporous silica nanoparticle-based stimuli-responsive capped drug delivery systems was carried out and applied to intracellular pH-Activated targeted cancer therapy [195].

Still in order to overcome the adverse reactions, toxicity and poor compliance from chemotherapy patients, a study was carried out aiming to develop an MSU-type mesoporous silica-based nanodevice able to selectively deliver bortezomib to folate receptor overexpressing multiple myeloma cells, improving therapeutic efficacy by localized drug delivery [196]. The inability to establish in vivo structure-activity relationships of nanoparticle-based drug delivery systems hampers the progress of research in this area, so the number of studies on evaluating by imaging and mathematical modeling the influence of surface chemistry, routes of administration and size of silica nanoparticles on drug biodistribution is gradually growing [197].

One of the main incentives for the use of mesoporous silica-based materials, especially in biotechnological applications, is their degradation in water. Although it has already been proven, there is still a lot of study to enhance and control silica dissolution in order to overcome the issue of bioaccumulation. For this purpose, a study proposed the introduction of imine groups into the silica framework and it promoted a rapid degradation both in neutral and acid aqueous solutions [198].

5.4 CO_2 Capture

Due to the growing world population and the accelerated economic development in all sectors, the world's energy consumption is growing proportionately and, considering that coal is still one of the main sources of energy in the world, CO_2 emissions are also increasing. Researchers anticipated that in 2050 the amount of CO_2 in the atmosphere will be a value close to 550 ppm and it may cause irreversible climatic disasters as well as a great impact on the global temperature [151, 199]. Despite all efforts to replace carbon-based energy with renewable energy, it is still unrealistic believe in a future world without coal burning and, hence, CO_2 emission [150].

The most adopted CO_2 capture system in large scale industry is liquid amine adsorption, which consists in the selective adsorption of CO_2 from a gas stream over liquid amine solvents, the most common being monoethanolamine (MEA) or diethanolamine (DEA) [151]. However, this method requires a large amount of heat for CO_2 desorption, which contributes to more than 50% of the operation costs [200]. Therefore, many CO_2 capture systems using solid sorbents are being studied and demonstrating to present several advantages [199]. The most investigated solid sorbents include alumina, metal organic frameworks (MOFs), zeolites, activated carbons and mesoporous silica [150].

MCM-41 modified with poly(ethyleneimine) (PEI) was synthesized for CO_2 capture and concluded that because of the chemical interaction between CO_2 molecules and PEI/MCM-41, a low regeneration ability of the materials at 40 °C is presented. Furthermore, PEI/MCM-41 loaded with 50 wt.% PEI exhibited the best potential for CO_2 capture due to the highest nitrogen content (17 wt.%) on the surface [152]. A hybrid 3-aminopropyltrimethoxysilane (APTS) and tetraethylenepentamine (TEPA) modified MCM-41 sorbent

were synthesized for CO_2 capture and it occurred successfully. The best proportion of matrix constituents was 30 wt.% APTS and 40 wt.% TEPA with maximum adsorption capacity of 3.50 mmol-CO_2/g-sorbent [151].

MCM-41 modified with monoethanolamine (MEA), benzylamine (BZA) and N-(2-aminoethyl)ethanolamine (AEEA) were synthesized for CO_2 capture. The materials exhibited satisfactory capture capacity, which were 102.98 mg/g, 39.96 mg/g and 64.69 mg/g for MCM-41-40%AEEA, MCM-41-40%BZA and MCM-41-50%MEA samples, respectively [201]. Amine functionalized large-pore MCM-41 and MCM-41 aluminosilicate (Si/Al = 15) were synthesized as supports for CO_2 capture. The amine/ MCM-41 aluminosilicate exhibited higher CO_2 capture capacity (more than 63% after 60 min of adsorption at 25 °C) and faster adsorption kinetics (71% faster after two minutes of adsorption at 25 °C) when compared with pure MCM-41 [206].

6 Conclusion

The great potential of silica-based mesoporous matrices, functionalized or not, was highlighted in this review paper. In recent decades, the literature has reported more and more the versatility and applicability of these materials on the most different scientific fronts such as adsorption, catalysis, CO_2 capture, bionanotechnology, enzyme immobilization, among others. There are many ways to obtain these molecular sieves and hydrothermal synthesis has gained relevance due to the possibility of using room temperature, short reaction times and cheap and environmentally friendly reagents.

The use of ionic liquids and ionic solids in the synthesis of silica-based mesoporous materials has shown to be promising. Its properties such as low vapor pressure, complex interactions between the molecules that compose them, non-detectable vapor pressure under normal conditions, the presence of an organic cation and an anion make these compounds suitable in a wide range of processing requirements. The functionalization of these molecular sieves with graphene is also being explored and is gaining ground in the scientific community. Both topics, the use of ionic liquids and solids and functionalization with graphene, are not conventional and there is still little about them reported in the literature. Therefore, this review is distinguished by focusing on these topics.

A challenge to be overcome by future research is the discovery of new ionic liquids and ionic solids which can be applied in the synthesis of silica-based mesoporous materials. In addition, there is still much to be explored regarding the incorporation of graphene in silica-based mesoporous materials and research must be carried out in order to further optimize these materials that already have unique structures and properties.

Author Contributions All authors contributed to the study conception and design. Material preparation, data collection and analysis were performed by Paloma Truccolo Reato, Adriele Sabrina Todero, Fabiana de Oliveira Pereira, Rogério Marcos Dallago, Katia Bernardo-Gusmão and Marcelo Luis Mignoni. The first draft of the manuscript was written by Paloma Truccolo Reato and all authors commented on previous versions of the manuscript. All authors read and approved the final manuscript.

Data Availability Not applicable.

Declarations

Ethical Approval Not applicable.

Consent to Participate All authors gave their consent to participate in the article (Marcelo L. Mignoni—on behalf of all co-authors).

Consent to Publish All authors gave their consent for publication of the article if it was accepted. (Marcelo L. Mignoni—on behalf of all co-authors).

Competing interests The authors have no relevant financial or non-financial interests to disclose.

References

1. Costa JAS, de Jesus RA, Santos DO et al (2020) Recent progresses in the adsorption of organic, inorganic, and gas compounds by MCM-41-based mesoporous materials. Microporous Mesoporous Mater 291:109698. https://doi.org/10.1016/j.micromeso.2019.109698
2. McBain JW (1933) The sorption of gases and vapours by solids. J Phys Chem 37:149–150. https://doi.org/10.1021/j150343a021
3. Luna FJ, Schuchardt U (2001) Modificação de zeólitas para uso em catálise. Quim Nova 24:885–892. https://doi.org/10.1590/S0100-40422001000600027
4. Vartuli JC, Schmitt KD, Kresge CT, Roth WJ, Leonowicz ME, McCullen SB, Hellring SDH, Beck JS, Schlenker JL, Olson DH, Sheppard EW (1994) Development of a formation mechanism for M41S materials. Stud Surf Sci Catal 84:53–60. https://doi.org/10.1016/S0167-2991(08)64096-3
5. Kresge CT, Vartuli JC, Roth WJ, Leonowicz ME (2004) The discovery of ExxonMobil's M41S family of mesoporous molecular sieves. Stud Surf Sci Catal 148:53–72. https://doi.org/10.1016/S0167-2991(04)80193-9
6. Kresge CT, Leonowicz ME, Roth WJ et al (1992) Ordered mesoporous molecular sieves synthesized by a liquid-crystal template mechanism. Nature 359:710–712. https://doi.org/10.1038/359710a0
7. BEHRENS P, (1997) Structure-directed materials syntheses: Synthesis field diagrams for the preparation of mesostructured silicas. Solid State Ion 101–103:255–260. https://doi.org/10.1016/S0167-2738(97)84039-8

8. Vartuli JC, Roth WJ, Beck JS et al (2001) The synthesis and properties of M41S and related mesoporous materials. Synthesis, molecular sieves, vol 1. Springer Berlin Heidelberg, Berlin, Heidelberg, pp 97–119. https://doi.org/10.1007/3-540-69615-6_4

9. Grela A, Kuc J, Bajda T (2021) A review on the application of zeolites and mesoporous silica materials in the removal of nonsteroidal anti-inflammatory drugs and antibiotics from water. Materials 14:4994. https://doi.org/10.3390/ma14174994

10. Głowniak S, Szczęśniak B, Choma J, Jaroniec M (2021) Advances in microwave synthesis of nanoporous materials. Adv Mater 33:2103477. https://doi.org/10.1002/adma.202103477

11. Kouznetsova T, Sauka J, Ivanets A (2021) Template synthesis and gas adsorption properties of ordered mesoporous aluminosilicates. Appl Nanosci 11:1903–1915. https://doi.org/10.1007/s13204-021-01871-y

12. Kumar MA, Krishna NV, Selvam P (2019) Novel ionic liquid-templated ordered mesoporous aluminosilicates: Synthesis, characterization and catalytic properties. Microporous Mesoporous Mater 275:172–179. https://doi.org/10.1016/j.micromeso.2018.08.033

13. Xu J, Luan Z, He H et al (1998) A reliable synthesis of cubic mesoporous MCM-48 molecular sieve. Chem Mater 10:3690–3698. https://doi.org/10.1021/cm980440d

14. Callister WD, Rethwisch DG (2016) Ciência e engenharia de materiais: uma introdução, 9th edn. LTC, Rio de Janeiro

15. Prasomsri T, Jiao W, Weng SZ, Garcia Martinez J (2015) Mesostructured zeolites: Bridging the gap between zeolites and MCM-41. Chem Commun 51:8900–8911. https://doi.org/10.1039/C4CC10391B

16. Schumacher K, Grün M, Unger KK (1999) Novel synthesis of spherical MCM-48. Microporous Mesoporous Mater 27:201–206. https://doi.org/10.1016/S1387-1811(98)00254-6

17. Chen C-Y, Burkett SL, Li H-X, Davis ME (1993) Studies on mesoporous materials II. Synthesis mechanism of MCM-41. Microporous Mater 2:27–34. https://doi.org/10.1016/0927-6513(93)80059-4

18. Schwanke AJ, Pergher SBC (2012) Peneiras moleculares mesoporosas MCM-41: Uma perspectiva histórica, o papel de cada reagente na síntese e sua caracterização básica. Perspectiva 36:113–125

19. Kumar D, Schumacher K, du Fresne von Hohenesche C et al (2001) MCM-41, MCM-48 and related mesoporous adsorbents: their synthesis and characterisation. Colloids Surf A Physicochem Eng Asp 187–188:109–116. https://doi.org/10.1016/S0927-7757(01)00638-0

20. Costa JAS, de Jesus RA, Santos DO et al (2021) Synthesis, functionalization, and environmental application of silica-based mesoporous materials of the M41S and SBA-n families: A review. J Environ Chem Eng 9:105259. https://doi.org/10.1016/j.jece.2021.105259

21. Peng R, Zhao D, Dimitrijevic NM et al (2012) Room temperature synthesis of Ti–MCM-48 and Ti–MCM-41 mesoporous materials and their performance on photocatalytic splitting of water. The Journal of Physical Chemistry C 116:1605–1613. https://doi.org/10.1021/jp210448v

22. Sigma-Aldrich (2021) Tetraethyl orthosilicate. Available in: https://www.sigmaaldrich.com/BR/pt/product/aldrich/86578. Accessed 22 Aug 2022

23. Sigma-Aldrich (2022) Tetramethyl orthosilicate. Available in: https://www.sigmaaldrich.com/BR/pt/product/aldrich/341436. Accessed 22 Aug 2022

24. Vartuli JC, Schmitt KD, Kresge CT et al (1994) Effect of surfactant/silica molar ratios on the formation of mesoporous molecular sieves: Inorganic mimicry of surfactant liquid-crystal phases and mechanistic implications. Chem Mater 6:2317–2326

25. Beck JS, Vartuli JC, Roth WJ et al (1992) A new family of mesoporous molecular sieves prepared with liquid crystal templates. J Am Chem Soc 114:470–475

26. Lin H-P, Liu S-B, Mou C-Y, Tang C-Y (1999) Hierarchical organization of mesoporous MCM-41 ropes. Chem Commun 7:583–584. https://doi.org/10.1039/a809767d

27. Park SS, Park JH, Park JH et al (2007) The preparation of fibrous MCM-41 using microwave heating. Key Eng Mater 336–338:1316–1319. https://doi.org/10.4028/www.scientific.net/KEM.336-338.1316

28. Li L, Yu S, Liu F et al (2005) Reactions of turpentine using Zr-MCM-41 family mesoporous molecular sieves. Catal Letters 100:227–233. https://doi.org/10.1007/s10562-005-3460-2

29. Prakash N, Balaji R, Chen S-M et al (2021) Investigation of template-assisted (MCM-41) mesoporous Co3O4 nanostructures and its superior supercapacitive retention. Vacuum 185:109998. https://doi.org/10.1016/j.vacuum.2020.109998

30. Sarı Yılmaz M, Dere Özdemir Ö, Pişkin S (2015) Synthesis and characterization of MCM-41 with different methods and adsorption of Sr2+ on MCM-41. Res Chem Intermed 41:199–211. https://doi.org/10.1007/s11164-013-1182-4

31. Costa JAS, Sarmento VHV, Romão LPC, Paranhos CM (2020) Removal of polycyclic aromatic hydrocarbons from aqueous media with polysulfone/MCM-41 mixed matrix membranes. J Memb Sci 601:117912. https://doi.org/10.1016/j.memsci.2020.117912

32. Dündar-Tekkaya E, Yürüm Y (2016) Synthesis of palladium incorporated MCM-41 via microwave irradiation and investigation of its hydrogen storage properties. Int J Hydrogen Energy 41:9828–9833. https://doi.org/10.1016/j.ijhydene.2016.03.047

33. Abbas SH, Adam F, Muniandy L (2020) Green synthesis of MCM-41 from rice husk and its functionalization with nickel(II) salen complex for the rapid catalytic oxidation of benzyl alcohol. Microporous Mesoporous Mater 305:110192. https://doi.org/10.1016/j.micromeso.2020.110192

34. Renuka NK, Praveen AK, Anas K (2013) Influence of CTAB molar ratio in tuning the texture of rice husk silica into MCM 41 and SBA-16. Mater Lett 109:70–73. https://doi.org/10.1016/j.matlet.2013.07.074

35. Vyshegorodtseva EV, Larichev YV, Mamontov GV (2019) The influence of CTAB/Si ratio on the textural properties of MCM-41 prepared from sodium silicate. J Solgel Sci Technol 92:496–505. https://doi.org/10.1007/s10971-019-05034-y

36. Wang L, Zhang J, Chen F (2009) Synthesis of hydrothermally stable MCM-48 mesoporous molecular sieve at low cost of CTAB surfactant. Microporous Mesoporous Mater 122:229–233. https://doi.org/10.1016/j.micromeso.2009.03.004

37. Bordin I, de Aguiar PV, Demaman Oro CE et al (2021) Nb-MCM-type mesoporous material synthesis using ionic solid as structure-directing agent for in situ lipase immobilization. Appl Biochem Biotechnol 193:1072–1085. https://doi.org/10.1007/s12010-020-03484-7

38. Pashaei M, Mehdipour E, Azaroon M (2019) Engineered mesoporous ionic-modified γ-Fe2O3@hydroxyapatite decorated with palladium nanoparticles and its catalytic properties in water. Appl Organomet Chem 33:e4622. https://doi.org/10.1002/aoc.4622

39. Lee H, Zones SI, Davis ME (2005) Zeolite synthesis using degradable structure-directing agents and pore-filling agents. J Phys Chem B 109:2187–2191. https://doi.org/10.1021/jp048908p

40. Gómez-Hortigüela L, Camblor MÁ (2017) Introduction to the zeolite structure-directing phenomenon by organic species: general aspects. Struct Bond 175:1–41. https://doi.org/10.1007/430_2017_8

41. Patuwan SZ, Arshad SE (2021) Important synthesis parameters affecting crystallization of zeolite T: A review. Materials 14:2890. https://doi.org/10.3390/ma14112890

42. Huang Z, Che S (2015) Fabrication of mesostructured silica materials through co-structure-directing route. Bull Chem Soc Jpn 88:617–632. https://doi.org/10.1246/bcsj.20140416

43. Zheng H, Gao C, Che S (2008) Amino and quaternary ammonium group functionalized mesoporous silica: An efficient ion-exchange method to remove anionic surfactant from AMS. Microporous Mesoporous Mater 116:299–307. https://doi.org/10.1016/j.micromeso.2008.04.016

44. Mignoni ML (2012) Zeólitas obtidas com líquidos iônicos como direcionadores de estrutura: síntese e reatividade. Universidade Federal do Rio Grande do Sul. Doctoral Thesis, p 168

45. Park JY, Han SW, Lee IH (2007) Preparation of electrospun porous ethyl cellulose fiber by THF/DMAc binary solvent system. J Ind Eng Chem 13:1002–1008

46. Konwarh R, Karak N, Misra M (2013) Electrospun cellulose acetate nanofibers: The present status and gamut of biotechnological applications. Biotechnol Adv 31:421–437. https://doi.org/10.1016/j.biotechadv.2013.01.002

47. Dupont J, Consorti CS, Spencer J (2000) Room temperature molten salts: neoteric "green" solvents for chemical reactions and processes. J Braz Chem Soc 11:337–344. https://doi.org/10.1590/S0103-50532000000400002

48. Wasserscheid P, Keim W (2000) Ionic Liquids - New aSolutionso for Transition Metal Catalysis. Angew Chem Int 39:3772–3789

49. Battiston CSZ, Ficanha AMM, Oro CED et al (2022) In situ calb enzyme immobilization in mesoporous material type MCM-48 synthesis using ionic solid [C14MI]Cl as structure-directing agent. Appl Biochem Biotechnol 194:748–761. https://doi.org/10.1007/s12010-021-03648-z

50. Philippi F, Welton T (2021) Targeted modifications in ionic liquids – from understanding to design. Phys Chem Chem Phys 23:6993–7021. https://doi.org/10.1039/D1CP00216C

51. Kianfar E, Mafi S (2020) Ionic liquids: properties, application, and synthesis. Fine Chem Eng 2:22–31. https://doi.org/10.37256/fce.212021693

52. Walden P (1914) Ueber die Molekulargrösse und elektrische Leitfähigkeit einiger geschmolzenen Salze. Bull Acad Imp Sci Saint-Petersbourg 8:405–422

53. Welton T (2018) Ionic liquids: A brief history. Biophys Rev 10:691–706. https://doi.org/10.1007/s12551-018-0419-2

54. Zhang M, Zhu W, Li H et al (2014) One-pot synthesis, characterization and desulfurization of functional mesoporous W-MCM-41 from POM-based ionic liquids. Chem Eng J 243:386–393. https://doi.org/10.1016/j.cej.2013.12.093

55. Mohamedali M, Ibrahim H, Henni A (2020) Imidazolium based ionic liquids confined into mesoporous silica MCM-41 and SBA-15 for carbon dioxide capture. Microporous Mesoporous Mater 294:109916. https://doi.org/10.1016/j.micromeso.2019.109916

56. de Aguiar Pedott V, Bordin I, dos Santos da Silva A et al (2020) Hierarchical pore structure of zeolite/MCM obtained by supramolecular templating using ionic liquid (C16MI·Cl) as the structure-directing agent. J Mater Sci 55:2343–2352. https://doi.org/10.1007/s10853-019-04117-z

57. Abbasi M, Pazuki G, Raisi A, Baghbanbashi M (2020) Thermophysical and rheological properties of sorbitol + ([mmim](MeO)2PO2) ionic liquid solutions: Solubility, density and viscosity. Food Chem 320:126566. https://doi.org/10.1016/j.foodchem.2020.126566

58. Aghaei A, Sobati MA (2022) Extraction of sulfur compounds from middle distillate fuels using ionic liquids and deep eutectic solvents: A critical review. Fuel 310:122279. https://doi.org/10.1016/j.fuel.2021.122279

59. Ibrahim MH, Hayyan M, Hashim MA, Hayyan A (2017) The role of ionic liquids in desulfurization of fuels: A review. Renew Sustain Energy Rev 76:1534–1549. https://doi.org/10.1016/j.rser.2016.11.194

60. Dyson P, Tilmann G (2005) Miscellaneous reactions. In: Metal catalysed reactions in ionic liquids: Catalysis by metal complexes, vol 29. Springer, Dordrech, pp 187–227. https://doi.org/10.1007/1-4020-3915-8_9

61. Miao L, Song Z, Zhu D et al (2021) Ionic liquids for supercapacitive energy storage: A mini-review. Energy Fuels 35:8443–8455. https://doi.org/10.1021/acs.energyfuels.1c00321

62. Sadjadi S (2021) Magnetic (poly) ionic liquids: A promising platform for green chemistry. J Mol Liq 323:114994. https://doi.org/10.1016/j.molliq.2020.114994

63. Araldi da Silva B, de Sousa Cunha R, Valério A et al (2021) Electrospinning of cellulose using ionic liquids: An overview on processing and applications. Eur Polym J 147:110283. https://doi.org/10.1016/j.eurpolymj.2021.110283

64. Wang Z, Yao Z, Zhou J, Zhang Y (2017) Reuse of waste cotton cloth for the extraction of cellulose nanocrystals. Carbohydr Polym 157:945–952. https://doi.org/10.1016/j.carbpol.2016.10.044

65. Dong K, Liu X, Dong H et al (2017) Multiscale studies on ionic liquids. Chem Rev 117:6636–6695. https://doi.org/10.1021/acs.chemrev.6b00776

66. Welton T (2004) Ionic liquids in catalysis. Coord Chem Rev 248:2459–2477. https://doi.org/10.1016/j.ccr.2004.04.015

67. Hashmi M, Sun Q, Tao J et al (2017) Comparison of autohydrolysis and ionic liquid 1-butyl-3-methylimidazolium acetate pretreatment to enhance enzymatic hydrolysis of sugarcane bagasse. Bioresour Technol 224:714–720. https://doi.org/10.1016/j.biortech.2016.10.089

68. Xiong R, Hameed N, Guo Q (2012) Cellulose/polycaprolactone blends regenerated from ionic liquid 1-butyl-3-methylimidazolium chloride. Carbohydr Polym 90:575–582. https://doi.org/10.1016/j.carbpol.2012.05.080

69. Cho C-W, Pham TPT, Zhao Y et al (2021) Review of the toxic effects of ionic liquids. Sci Total Environ 786:147309. https://doi.org/10.1016/j.scitotenv.2021.147309

70. Rogers RD, Seddon KR (2003) Ionic liquids–solvents of the future? Science (1979) 302:792–793. https://doi.org/10.1126/science.1090313

71. Seitkalieva MM, Samoylenko DE, Lotsman KA et al (2021) Metal nanoparticles in ionic liquids: Synthesis and catalytic applications. Coord Chem Rev 445:213982. https://doi.org/10.1016/j.ccr.2021.213982

72. Sanaeishoar H, Sabbaghan M, Mohave F (2015) Synthesis and characterization of micro-mesoporous MCM-41 using various ionic liquids as co-templates. Microporous Mesoporous Mater 217:219–224. https://doi.org/10.1016/j.micromeso.2015.06.027

73. Sanaeishoar H, Sabbaghan M, Ghazvini M et al (2022) Manufacturing porous materials using dabco-based ionic liquid. SILICON 14:6291–6297. https://doi.org/10.1007/s12633-021-01403-x

74. Li D, Min H, Jiang X et al (2013) One-pot synthesis of Aluminum-containing ordered mesoporous silica MCM-41 using coal fly ash for phosphate adsorption. J Colloid Interface Sci 404:42–48. https://doi.org/10.1016/j.jcis.2013.04.018

75. González Vargas OA, de los Reyes Heredia JA, Montesinos Castellanos A et al (2013) Cerium incorporating into MCM-41 mesoporous materials for CO oxidation. Mater Chem Phys 139:125–133. https://doi.org/10.1016/j.matchemphys.2012.12.081

76. Li X, Li B, Xu J et al (2010) Synthesis and characterization of Ln-ZSM-5/MCM-41 (Ln = La, Ce) by using kaolin as raw material. Appl Clay Sci 50:81–86. https://doi.org/10.1016/j.clay.2010.07.006

77. Oliveira AC, Rangel M do C, Fierro JLG et al (2005) Efeito do cromo nas propriedades catalíticas da MCM-41. Quim Nova 28:37–41.https://doi.org/10.1590/S0100-40422005000100007

78. Brezoiu A-M, Deaconu M, Nicu I et al (2019) Heteroatom modified MCM-41-silica carriers for Lomefloxacin delivery systems. Microporous Mesoporous Mater 275:214–222. https://doi.org/10.1016/j.micromeso.2018.08.031

79. Xin H, Ke T (2016) Preparation and adsorption denitrogenation from model fuel or diesel oil of heteroatoms mesoporous molecular sieve Co-MCM-41. Energy Sources A: Recovery Util Environ Eff 38:2560–2567. https://doi.org/10.1080/15567036.2015.1062823

80. Reddy JK, Mantri K, Lad S et al (2020) Synthesis of Ce-MCM-22 and its enhanced catalytic performance for the removal of olefins from aromatic stream. J Porous Mater 27:1649–1658. https://doi.org/10.1007/s10934-020-00940-x

81. Das DR, Kalita P, Talukdar AK (2020) Ti/Cr incorporated mesoporous MCM-48 for oxidation of styrene to benzaldehyde. J Porous Mater 27:893–903. https://doi.org/10.1007/s10934-020-00868-2

82. Zhang X, Du T (2022) Study of rice husk ash derived MCM-41-type materials on pore expansion, Al incorporation, PEI impregnation, and CO2 adsorption. Korean J Chem Eng 39:736–759. https://doi.org/10.1007/s11814-021-0904-3

83. Liang T, Chen J, Wang S et al (2022) Conversion of methanol to hydrocarbons over H-MCM-22 zeolite: deactivation behaviours related to acid density and distribution. Catal Sci Technol. https://doi.org/10.1039/D2CY01270G

84. Atchudan R, Pandurangan A, Joo J (2013) Synthesis of multilayer graphene balls on mesoporous Co-MCM-41 molecular sieves by chemical vapour deposition method. Microporous Mesoporous Mater 175:161–169. https://doi.org/10.1016/j.micromeso.2013.03.035

85. Yu W, Sisi L, Haiyan Y, Jie L (2020) Progress in the functional modification of graphene/graphene oxide: a review. RSC Adv 10:15328–15345. https://doi.org/10.1039/D0RA01068E

86. Novoselov KS, Geim AK, Morozov SV et al (2004) Electric Field Effect in Atomically Thin Carbon Films. Science (1979) 306:666–669. https://doi.org/10.1126/science.1102896

87. Olabi AG, Abdelkareem MA, Wilberforce T, Sayed ET (2021) Application of graphene in energy storage device – A review. Renew Sustain Energy Rev 135:110026. https://doi.org/10.1016/j.rser.2020.110026

88. Feng X, Yan Z, Chen N et al (2013) Synthesis of a graphene/polyaniline/MCM-41 nanocomposite and its application as a supercapacitor. New J Chem 37:2203. https://doi.org/10.1039/c3nj00108c

89. Zhang Y, Tan Y-W, Stormer HL, Kim P (2005) Experimental observation of the quantum Hall effect and Berry's phase in graphene. Nature 438:201–204. https://doi.org/10.1038/nature04235

90. Geim AK (2009) Graphene: Status and Prospects. Science (1979) 324:1530–1534. https://doi.org/10.1126/science.1158877

91. Novoselov KS, Jiang Z, Zhang Y et al (2007) Room-temperature quantum hall effect in graphene. Science (1979) 315:1379–1379.https://doi.org/10.1126/science.1137201

92. Wu S, Ge R, Lu M et al (2015) Graphene-based nano-materials for lithium–sulfur battery and sodium-ion battery. Nano Energy 15:379–405. https://doi.org/10.1016/j.nanoen.2015.04.032

93. Xu Y, Shi G, Duan X (2015) Self-assembled three-dimensional graphene macrostructures: Synthesis and applications in supercapacitors. Acc Chem Res 48:1666–1675. https://doi.org/10.1021/acs.accounts.5b00117

94. Fan X, Zhang G, Zhang F (2015) Multiple roles of graphene in heterogeneous catalysis. Chem Soc Rev 44:3023–3035. https://doi.org/10.1039/C5CS00094G

95. Sun X, Liu Z, Welsher K et al (2008) Nano-graphene oxide for cellular imaging and drug delivery. Nano Res 1:203–212. https://doi.org/10.1007/s12274-008-8021-8

96. Huang H, Ying Y, Peng X (2014) Graphene oxide nanosheet: an emerging star material for novel separation membranes. J Mater Chem A 2:13772–13782. https://doi.org/10.1039/C4TA02359E

97. Georgakilas V, Tiwari JN, Kemp KC et al (2016) Noncovalent functionalization of graphene and graphene oxide for energy materials, biosensing, catalytic, and biomedical applications. Chem Rev 116:5464–5519. https://doi.org/10.1021/acs.chemrev.5b00620

98. Yang Z, Tian J, Yin Z et al (2019) Carbon nanotube- and graphene-based nanomaterials and applications in high-voltage supercapacitor: A review. Carbon N Y 141:467–480. https://doi.org/10.1016/j.carbon.2018.10.010

99. Sengupta J, Hussain CM (2021) Graphene-based field-effect transistor biosensors for the rapid detection and analysis of viruses: A perspective in view of COVID-19. Carbon Trends 2:100011. https://doi.org/10.1016/j.cartre.2020.100011

100. Chen B, Zhong X, Zhou G et al (2022) Graphene-supported atomically dispersed metals as bifunctional catalysts for next-generation batteries based on conversion reactions. Adv Mater 34:2105812. https://doi.org/10.1002/adma.202105812

101. Su H, Hu YH (2021) Recent advances in graphene-based materials for fuel cell applications. Energy Sci Eng 9:958–983. https://doi.org/10.1002/ese3.833

102. Mahalingam S, Manap A, Omar A et al (2021) Functionalized graphene quantum dots for dye-sensitized solar cell: Key challenges, recent developments and future prospects. Renew Sustain Energy Rev 144:110999. https://doi.org/10.1016/j.rser.2021.110999

103. Lin L, Peng H, Liu Z (2019) Synthesis challenges for graphene industry. Nat Mater 18:520–524. https://doi.org/10.1038/s41563-019-0341-4

104. Razaq A, Bibi F, Zheng X et al (2022) Review on graphene-, graphene oxide-, reduced graphene oxide-based flexible composites: From fabrication to applications. Materials 15:1012. https://doi.org/10.3390/ma15031012

105. Finkler DE, Mignoni ML, Oro CED, Dallago RM, Reato PT (2022) Método de preparação do material mesoporoso MRD-1, um grafenosilicato possuindo topologia MCM, utilizando como agente direcionador de estrutura um sólido iônico. Depositor: Diana Exenberger Finkler. Procurador: Custodio Cesar Castro de Almeida. BR 10 2022 008344 4. Deposit: 29 Apr 2022

106. Finkler DE, Pereira F de O, Mignoni ML, Todero AS, Dallago RM (2022) Método de preparação do material mesoporoso MRD-2, um grafenosilicato dopado com nióbio possuindo topologia MCM, utilizando um sólido iônico como agente direcionador. Depositor: Diana Exenberger Finkler. Procurador: Custodio Cesar Castro de Almeida. BR 102022010583-9 A2. Deposit: 31 May 2022

107. Finkler DE, Todero AS, Pereira F de O, Reato PT, Mignoni ML, Dallago RM (2022) Método de preparação do material mesoporoso MRD-3, um grafenosilicato dopado com TiO2 possuindo topologia MCM, utilizandoum sólido iônico como agente direcionador. Depositor: Diana Exenberger Finkler. Procurador: Custodio Cesar Castro de Almeida. BR 10 2022 015137 7. Deposit: 29 July 2022.

108. Finkler DE, Todero AS, Pereira FO, Mignoni ML, Reato PT, Dallago RM (2022) Método de preparação do material mesoporoso MRD-4, um grafenosilicato dopado com ZnO possuindo topologia MCM, utilizando um sólido iônico como agente direcionador. Depositor: Diana Exenberger Finkler. Procurador: Custodio Cesar Castro de Almeida. BR 10 2022 019561 7. Deposit: 29 Sep 2022

109. Finkler DE, Todero AS, Pereira FO, Mignoni ML, Reato PT, Dallago RM (2022) Processo de síntese do material mesoporoso MRD-5, um grafenosilicato dopado com FeO possuindo topologia MCM, utilizando um sólido iônico como agente direcionador de estrutura. Depositor: Diana Exenberger Finkler. Procurator: Custodio Cesar Castro de Almeida. BR 10 2022 021836 6. Deposit: 27 Oct 2022

110. Finkler DE, Todero AS, Pereira FO, Reato PT, Mignoni ML, Dallago RM (2022) Processo de síntese do material MRD-6, um grafenosilicato mesoporoso dopado com alumínio possuindo topologia MCM, utilizando o sólido iônico [$C_{16}MI$].Cl como agente direcionador de estrutura. Depositor: Diana Exenberger Finkler. Procurator: Custodio Cesar Castro de Almeida. BR 10 2022 022785 3. Deposit: 09 Nov 2022

111. Azaroff LV, Wilson AJC (1968) Elements of X-ray Crystallography, 2nd edn. McGraw-Hill Inc., New York

112. Napolitano HB, Camargo AJ, Mascarenhas YP et al (2007) Análise da difração dos Raios X. Rev Process Quím 1:35–45. https://doi.org/10.19142/rpq.v01i01.p35-45.2007

113. Cunha S (2008) Métodos simples de formação de monocristal de substância orgânica para estudo estrutural por difração de raios X. Quim Nova 31:906–909. https://doi.org/10.1590/S0100-40422008000400031

114. Mould RF (1995) The early history of X-ray diagnosis with emphasis on the contributions of physics 1895–1915. Phys Med Biol 40:1741–1787. https://doi.org/10.1088/0031-9155/40/11/001

115. Friedrich W, Knipping P, Laue MV (1913) Interferenzerscheinungen bei Röntgenstrahlen. Sitzungsberichte der mathematisch-physikalischen Klasse der Bayerischen Akademie der Wissenschaften München 346:971–988. https://doi.org/10.1002/andp.19133461004

116. Laue MV (1912) Eine quantitative Prüfung der Theorie für die InterferenzErscheinungen bei Röntgenstrahlen. Sitzungsberichte der mathematischphysikalischen Klasse der Bayerischen Akademie der Wissenschaften München 39:368–372. https://doi.org/10.1002/andp.19133461005

117. Cowley JM (1995) Diffraction physics, 3rd edn. North Holland, Amsterdam

118. Wilkins SW (2013) Celebrating 100 years of X-ray crystallography. Acta Crystallogr A 69:1–4. https://doi.org/10.1107/S0108767312048490

119. Thommes M, Kaneko K, Neimark AV et al (2015) Physisorption of gases, with special reference to the evaluation of surface area and pore size distribution (IUPAC Technical Report). Pure Appl Chem 87:1051–1069. https://doi.org/10.1515/pac-2014-1117

120. Cullity BD, Stock SR (1956) Elements of X-ray diffraction. Pearson, London

121. Guinier A (1952) X-ray crystallographic technology. Acta Cryst 6:751–752. https://doi.org/10.1107/S0365110X53002143

122. Bae Y-S, Yazaydın AÖ, Snurr RQ (2010) Evaluation of the BET method for determining surface areas of MOFs and zeolites that contain ultra-micropores. Langmuir 26:5475–5483. https://doi.org/10.1021/la100449z

123. Teixeira VG, Coutinho FMB, Gomes AS (2001) Principais métodos de caracterização da porosidade de resinas à base de divinilbenzeno. Quim Nova 24:808–818. https://doi.org/10.1590/S0100-40422001000600019

124. Ambroz F, Macdonald TJ, Martis V, Parkin IP (2018) Evaluation of the BET theory for the characterization of meso and microporous MOFs. Small Methods 2:1800173. https://doi.org/10.1002/smtd.201800173

125. Maximov MA, Galukhin AV, Gor GY (2019) Pore-Size Distribution of Silica Colloidal Crystals from Nitrogen Adsorption Isotherms. Langmuir 35:14975–14982. https://doi.org/10.1021/acs.langmuir.9b02252

126. Delgado Mons R, Cornette V, Toso JP et al (2019) Effects of potential models on nitrogen adsorption on triangular pore: An improved mixed model for energetic characterization of activated carbon. Appl Surf Sci 481:1035–1043. https://doi.org/10.1016/j.apsusc.2019.02.201

127. Alshameri A, He H, Zhu J et al (2018) Adsorption of ammonium by different natural clay minerals: Characterization, kinetics and adsorption isotherms. Appl Clay Sci 159:83–93. https://doi.org/10.1016/j.clay.2017.11.007

128. Fagerlund G (1973) Determination of specific surface by the BET method. Matér Construct 6:239–245. https://doi.org/10.1007/BF02479039

129. Dedavid BA, Gomes CI, Machado G (2007) Microscopia Eletrônica de Varredura: aplicações e preparação de amostras: materiais poliméricos, metálicos e semicondutores. EDIPUCRS, Porto Alegre

130. Ural N (2021) The significance of scanning electron microscopy (SEM) analysis on the microstructure of improved clay: An overview. Open Geosciences 13:197–218. https://doi.org/10.1515/geo-2020-0145

131. Bogner A, Jouneau P-H, Thollet G et al (2007) A history of scanning electron microscopy developments: Towards "wet-STEM" imaging. Micron 38:390–401. https://doi.org/10.1016/j.micron.2006.06.008

132. Goldstein JI, Newbury DE, Echlin P et al (1993) Scanning electron microscopy and X-ray microanalysis. A text for biologists, materials scientists, and geologists. Geol Mag 130:402–403. https://doi.org/10.1017/S0016756800020276

133. Williams DB, Carter CB (2009) Transmission electron microscopy. Springer US, Boston

134. Reimer L (2013) Transmission electron microscopy: Physics of image formation and microanalysis. Springer

135. Kestenbach HJ, Bota Filho WJ (1994) Microscopia eletrônica de transmissão e varredura. São Paulo: Associação Brasileira de Metais

136. Cavalheiro ÉTG, Ionashiro M, Breviglieri ST et al (1995) A influência de fatores experimentais nos resultados de análises termogravimétricas. Quim Nova 18:305–308

137. Brown ME (2004) Introduction to thermal analysis. Kluwer Academic Publishers, Dordrecht

138. Saadatkhah N, Carillo Garcia A, Ackermann S et al (2020) Experimental methods in chemical engineering: Thermogravimetric analysis—TGA. Can J Chem Eng 98:34–43. https://doi.org/10.1002/cjce.23673

139. Gabbot P (2008) Principles and applications of thermal analysis. John Wiley & Sons

140. Menczel JD, Prime RB (2009) Thermal analysis of polymers, fundamentals and applications. John Wiley & Sons

141. Fabris HJ (1978) Thermal and oxidative stability of urethanes. Adv Urethane Sci Technol 6:173–196

142. Chattopadhyay DK, Webster DC (2009) Thermal stability and flame retardancy of polyurethanes. Prog Polym Sci 34:1068–1133. https://doi.org/10.1016/j.progpolymsci.2009.06.002

143. Bhattacharyya S, Lelong G, Saboungi M-L (2006) Recent progress in the synthesis and selected applications of MCM-41: a short review. J Exp Nanosci 1:375–395. https://doi.org/10.1080/17458080600812757

144. Martínez-Edo G, Balmori A, Pontón I et al (2018) Functionalized ordered mesoporous silicas (MCM-41): Synthesis and applications in catalysis. Catalysts 8:617. https://doi.org/10.3390/catal8120617

145. Chen P, Zhang Q, Shu R et al (2017) Catalytic depolymerization of the hydrolyzed lignin over mesoporous catalysts. Bioresour Technol 226:125–131. https://doi.org/10.1016/j.biortech.2016.12.030

146. Xu J, Yang Y, Liu B et al (2022) Ultrasonic assisted enhanced catalytic effect of perovskite to promote depolymerization of lignin. Int J Biol Macromol 218:431–438. https://doi.org/10.1016/j.ijbiomac.2022.07.120

147. Du B, Chen C, Sun Y et al (2020) Efficient and controllable ultrasound-assisted depolymerization of organosolv lignin catalyzed to liquid fuels by MCM-41 supported phosphotungstic acid. RSC Adv 10:31479–31494. https://doi.org/10.1039/D0RA05069E

148. Klamrassamee T, Laosiripojana N, Cronin D et al (2015) Effects of mesostructured silica catalysts on the depolymerization of organosolv lignin fractionated from woody eucalyptus. Bioresour Technol 180:222–229. https://doi.org/10.1016/j.biortech.2014.12.098

149. Loganathan S, Tikmani M, Ghoshal AK (2013) Novel pore-expanded MCM-41 for CO2 capture: Synthesis and characterization. Langmuir 29:3491–3499. https://doi.org/10.1021/la400109j

150. Wang X, Chen L, Guo Q (2015) Development of hybrid amine-functionalized MCM-41 sorbents for CO2 capture. Chem Eng J 260:573–581. https://doi.org/10.1016/j.cej.2014.08.107

151. Le Thi MU, Lee S-Y, Park S-J (2014) Preparation and characterization of PEI-loaded MCM-41 for CO2 capture. Int J Hydrogen Energy 39:12340–12346. https://doi.org/10.1016/j.ijhydene.2014.04.112

152. Yang S-T, Kim J-Y, Kim J, Ahn W-S (2012) CO2 capture over amine-functionalized MCM-22, MCM-36 and ITQ-2. Fuel 97:435–442. https://doi.org/10.1016/j.fuel.2012.03.034

153. Wang X, Guo Q, Kong T (2015) Tetraethylenepentamine-modified MCM-41/silica gel with hierarchical mesoporous structure for CO2 capture. Chem Eng J 273:472–480. https://doi.org/10.1016/j.cej.2015.03.098

154. Ulu A, Ozcan I, Koytepe S, Ates B (2018) Design of epoxy-functionalized Fe3O4@MCM-41 core–shell nanoparticles for enzyme immobilization. Int J Biol Macromol 115:1122–1130. https://doi.org/10.1016/j.ijbiomac.2018.04.157

155. Yasutaka K, Takato Y, Takashi K et al (2011) Enhancement in adsorption and catalytic activity of enzymes immobilized on phosphorus- and calcium-modified MCM-41. J Phys Chem B 115:10335–10345. https://doi.org/10.1021/jp203632g

156. Calgaroto C, Scherer RP, Calgaroto S et al (2011) Immobilization of porcine pancreatic lipase in zeolite MCM 22 with different Si/Al ratios. Appl Catal A Gen 394:101–104. https://doi.org/10.1016/j.apcata.2010.12.032

157. Zeng W, Qian X-F, Zhang Y-B et al (2005) Organic modified mesoporous MCM-41 through solvothermal process as drug delivery system. Mater Res Bull 40:766–772. https://doi.org/10.1016/j.materresbull.2005.02.011

158. Delle Piane M, Corno M, Pedone A et al (2014) Large-scale B3LYP simulations of ibuprofen adsorbed in MCM-41 mesoporous silica as drug delivery system. J Phys Chem C 118:26737–26749. https://doi.org/10.1021/jp507364h

159. Shariatinia Z, Zahraee Z (2017) Controlled release of metformin from chitosan–based nanocomposite films containing mesoporous MCM-41 nanoparticles as novel drug delivery systems. J Colloid Interface Sci 501:60–76. https://doi.org/10.1016/j.jcis.2017.04.036

160. Oliveira DM, Andrada AS (2019) Synthesis of ordered mesoporous silica MCM-41 with controlled morphology for potential application in controlled drug delivery systems. Cerâmica 65:170–179. https://doi.org/10.1590/0366-69132019653742509

161. Machado SWM, Santana JC, Pedrosa AMG et al (2018) Catalytic cracking of isopropylbenzene over hybrid HZSM-12/M41S (M41S = MCM-41 or MCM-48) micro-mesoporous materials. Pet Sci Technol 36:923–929. https://doi.org/10.1080/10916466.2018.1454950

162. Čapek L, Adam J, Grygar T et al (2008) Oxidative dehydrogenation of ethane over vanadium supported on mesoporous materials of M41S family. Appl Catal A Gen 342:99–106. https://doi.org/10.1016/j.apcata.2008.03.003

163. Şimşek V, Mürtezaoğlu K (2018) Characterizations and catalytic activities investigation of synthesized solid-based heterogeneous catalysts in the esterification reaction. Anadolu Univ J Sci Technol-A Appl Sci Eng 19:422–432. https://doi.org/10.18038/aubtda.357270

164. Ehiro T, Itagaki A, Misu H et al (2016) Effects of acid treatment on the acidic properties and catalytic activity of MCM-41 for the oxidative dehydrogenation of isobutane. J Chem Eng Jpn 49:152–160. https://doi.org/10.1252/jcej.15we155

165. Goldsmith BR, Esterhuizen J, Liu J et al (2018) Machine learning for heterogeneous catalyst design and discovery. AIChE J 64:2311–2323. https://doi.org/10.1002/aic.16198

166. Ziolek M (2004) Catalytic liquid-phase oxidation in heterogeneous system as green chemistry goal—advantages and disadvantages of MCM-41 used as catalyst. Catal Today 90:145–150. https://doi.org/10.1016/j.cattod.2004.04.020

167. Taherian Z, Khataee A, Orooji Y (2020) Facile synthesis of yttria-promoted nickel catalysts supported on MgO-MCM-41 for syngas production from greenhouse gases. Renew Sustain Energy Rev 134:110130. https://doi.org/10.1016/j.rser.2020.110130

168. Eslami M, Dekamin MG, Motlagh L, Maleki A (2018) MCM-41 mesoporous silica: a highly efficient and recoverable catalyst for rapid synthesis of α-aminonitriles and imines. Green Chem Lett Rev 11:36–46. https://doi.org/10.1080/17518253.2017.1421269

169. Naik SP, Bui V, Ryu T et al (2010) Al-MCM-41 as methanol dehydration catalyst. Appl Catal A Gen 381:183–190. https://doi.org/10.1016/j.apcata.2010.04.007

170. Arora S, Gosu V, Kumar UKA, Subbaramaiah V (2021) Valorization of glycerol into glycerol carbonate using the stable heterogeneous catalyst of Li/MCM-41. J Clean Prod 295:126437. https://doi.org/10.1016/j.jclepro.2021.126437

171. Polikarpova P, Akopyan A, Shigapova A et al (2018) Oxidative desulfurization of fuels using heterogeneous catalysts based on MCM-41. Energy Fuels 32:10898–10903. https://doi.org/10.1021/acs.energyfuels.8b02583

172. Du B, Chen C, Sun Y et al (2020) Catalytic conversion of lignin to bio-oil over PTA/MCM-41 catalyst assisted by ultrasound acoustic cavitation. Fuel Process Technol 206:106479. https://doi.org/10.1016/j.fuproc.2020.106479

173. Sikarwar P, Kumar UKA, Gosu V, Subbaramaiah V (2018) Catalytic oxidative desulfurization of DBT using green catalyst (Mo/MCM-41) derived from coal fly ash. J Environ Chem Eng 6:1736–1744. https://doi.org/10.1016/j.jece.2018.02.021

174. Díaz JF, Balkus KJ (1996) Enzyme immobilization in MCM-41 molecular sieve. J Mol Catal B Enzym 2:115–126. https://doi.org/10.1016/S1381-1177(96)00017-3

175. Cao S, Xu P, Ma Y et al (2016) Recent advances in immobilized enzymes on nanocarriers. Chin J Catal 37:1814–1823. https://doi.org/10.1016/S1872-2067(16)62528-7

176. Ma H, He J, Evans DG, Duan X (2004) Immobilization of lipase in a mesoporous reactor based on MCM-41. J Mol Catal B Enzym 30:209–217. https://doi.org/10.1016/j.molcatb.2004.04.007

177. Casadonte F, Pasqua L, Savino R, Terracciano R (2010) Smart trypsin adsorption into N-(2-Aminoethyl)-3-aminopropyl-modified mesoporous silica for ultra fast protein digestion. Chem Eur J 16:8998–9001. https://doi.org/10.1002/chem.201000120

178. Yu D, Zhang X, Wang T et al (2021) Immobilized Candida antarctica lipase B (CALB) on functionalized MCM-41: Stability

and catalysis of transesterification of soybean oil and phytosterol. Food Biosci 40:100906. https://doi.org/10.1016/j.fbio.2021.100906

179. Vallet-Regi M, Rámila A, del Real RP, Pérez-Pariente J (2001) A New Property of MCM-41: drug delivery system. Chem Mater 13:308–311. https://doi.org/10.1021/cm0011559

180. Xu Q, Yang Y, Lu J et al (2022) Recent trends of mesoporous silica-based nanoplatforms for nanodynamic therapies. Coord Chem Rev 469:214687. https://doi.org/10.1016/j.ccr.2022.214687

181. Mazzotta E, de Santo M, Lombardo D et al (2022) Mesoporous silicas in materials engineering: Nanodevices for bionanotechnologies. Mater Today Bio 17:100472. https://doi.org/10.1016/j.mtbio.2022.100472

182. Escriche-Navarro B, Escudero A, Lucena-Sánchez E et al (2022) Mesoporous silica materials as an emerging tool for cancer immunotherapy. Adv Sci 9:2200756. https://doi.org/10.1002/advs.202200756

183. Escudero A, Carrillo-Carrión C, Castillejos MC et al (2021) Photodynamic therapy: photosensitizers and nanostructures. Mater Chem Front 5:3788–3812. https://doi.org/10.1039/D0QM00922A

184. Wang K, Lu J, Li J et al (2021) Current trends in smart mesoporous silica-based nanovehicles for photoactivated cancer therapy. J Control Release 339:445–472. https://doi.org/10.1016/j.jconrel.2021.10.005

185. Xu Z, Ma X, Gao Y-E et al (2017) Multifunctional silica nanoparticles as a promising theranostic platform for biomedical applications. Mater Chem Front 1:1257–1272. https://doi.org/10.1039/C7QM00153C

186. Horcajada P, Rámila A, Pérez-Pariente J, Vallet-Regí M (2004) Influence of pore size of MCM-41 matrices on drug delivery rate. Microporous Mesoporous Mater 68:105–109. https://doi.org/10.1016/j.micromeso.2003.12.012

187. Vyskočilová E, Luštická I, Paterová I et al (2014) Modified MCM-41 as a drug delivery system for acetylsalicylic acid. Solid State Sci 38:85–89. https://doi.org/10.1016/j.solidstatesciences.2014.10.004

188. Manzano M, Aina V, Areán CO et al (2008) Studies on MCM-41 mesoporous silica for drug delivery: Effect of particle morphology and amine functionalization. Chem Eng J 137:30–37. https://doi.org/10.1016/j.cej.2007.07.078

189. Pajchel L, Kolodziejski W (2018) Synthesis and characterization of MCM-48/hydroxyapatite composites for drug delivery: Ibuprofen incorporation, location and release studies. Mater Sci Eng, C 91:734–742. https://doi.org/10.1016/j.msec.2018.06.028

190. Popova T, Tzankov B, Voycheva C et al (2021) Mesoporous silica MCM-41 and HMS as advanced drug delivery carriers for bicalutamide. J Drug Deliv Sci Technol 62:102340. https://doi.org/10.1016/j.jddst.2021.102340

191. Galhano J, Marcelo GA, Duarte MP, Oliveira E (2022) Ofloxacin@Doxorubicin-Epirubicin functionalized MCM-41 mesoporous silica–based nanocarriers as synergistic drug delivery tools for cancer related bacterial infections. Bioorg Chem 118:105470. https://doi.org/10.1016/j.bioorg.2021.105470

192. García-Fernández A, Sancenón F, Martínez-Máñez R (2021) Mesoporous silica nanoparticles for pulmonary drug delivery. Adv Drug Deliv Rev 177:113953. https://doi.org/10.1016/j.addr.2021.113953

193. García-Fernández A, Sancho M, Bisbal V et al (2021) Targeted-lung delivery of dexamethasone using gated mesoporous silica nanoparticles. A new therapeutic approach for acute lung injury treatment. J Control Release 337:14–26. https://doi.org/10.1016/j.jconrel.2021.07.010

194. Zhang Y, Wang W, Zhang Y et al (2018) "Three-in-one" multifunctional gatekeeper gated mesoporous silica nanoparticles for intracellular pH-activated targeted cancer therapy. ACS Appl Bio Mater 1:572–580. https://doi.org/10.1021/acsabm.8b00050

195. de Santo M, Giovinazzo A, Fava M et al (2023) Engineered mesoporous silica-based nanoparticles as smart chemotherapy nanodevice for bortezomib administration. Mater Chem Front 7:216–229. https://doi.org/10.1039/D2QM01009G

196. Dogra P, Adolphi NL, Wang Z et al (2018) Establishing the effects of mesoporous silica nanoparticle properties on in vivo disposition using imaging-based pharmacokinetics. Nat Commun 9:4551. https://doi.org/10.1038/s41467-018-06730-z

197. Travaglini L, Picchetti P, Totovao R et al (2019) Highly degradable imine-doped mesoporous silica particles. Mater Chem Front 3:111–119. https://doi.org/10.1039/C8QM00438B

198. Lee D, Jin Y, Jung N et al (2011) Gravimetric analysis of the adsorption and desorption of CO_2 on amine-functionalized mesoporous silica mounted on a microcantilever array. Environ Sci Technol 45:5704–5709. https://doi.org/10.1021/es200680v

199. Zhang X, Zhu Z, Sun X et al (2019) Reducing energy penalty of CO2 capture using Fe promoted SO42–/ZrO2/MCM-41 catalyst. Environ Sci Technol 53:6094–6102. https://doi.org/10.1021/acs.est.9b01901

200. Mukherjee S, Akshay SAN (2019) Amine-impregnated MCM-41 in post-combustion CO2 capture: Synthesis, characterization, isotherm modelling. Adv Powder Technol 30:3231–3240. https://doi.org/10.1016/j.apt.2019.09.032

201. Jahandar Lashaki M, Ziaei-Azad H, Sayari A (2022) Unprecedented improvement of the hydrothermal stability of amine-grafted MCM-41 silica for CO2 capture via aluminum incorporation. Chem Eng J 450:138393. https://doi.org/10.1016/j.cej.2022.138393